**Evidence for Deformation and Faulting in the Muckleshoot basin, Washington State**

by

Justin Hamilton Cox

A thesis submitted to the Graduate Faculty of
Auburn University
in partial fulfillment of the
requirements for the Degree of
Master of Science

Auburn, Alabama
May 10, 2015



Approved by

Lorraine W. Wolf, Chair, Professor of Geosciences
Mark G. Steltenpohl, Professor of Geosciences
Ming-Kuo Lee, Professor of Geosciences

## Abstract

The Muckleshoot basin of Western Washington state extends from the western base of the Cascades to approximately 10 km east of the Puget Sound. Mapped traces of the Tacoma and White River fault systems, to the west and southeast, respectively, stop abruptly at the basin margins, where sediments cover the underlying structures recorded in deeper strata. This research presents new crustal models based on analyses of gravity and magnetic data and explores possible connectivity of mapped faults to the east and west of the basin. As discussed in previous studies, the Muckleshoot basin appears to be segmented into two smaller basins by a northwest-southeast-trending gravity high that runs roughly parallel to the trend of the White River fault. Gravity and magnetic anomaly maps created in this study support the existence of the two sub-basins and explore any structural control over the location of the two. Two-dimensional cross-sectional models indicate the sub-basins are approximately 20 km wide and have Eocene-aged sediments buried up to roughly eight to nine km below the surface. Deformation of Quaternary sediments suggests that the basin is actively deforming today as a consequence of plate subduction to the west. Pseudo-three-dimensional models constructed from three intersecting profiles extracted from the gravity and magnetic data indicate that the White River fault bends slightly to the west, aligning with a splay of the Tacoma fault. This geometry is consistent with north-directed compression and clockwise rotation postulated from geodetic models. The geometry revealed in the models raises the potential for an interacting fault system in which rupture along one segment could trigger or advance failure on another.

## Acknowledgments

First and foremost I would like to thank my thesis advisor, Dr. Lorraine Wolf for her support throughout this entire project. The patience, devotion and compassion she showed me during my time at Auburn will always be remembered. I could not have done this without her. I would also like to thank my committee members Dr. Mark Steltenpohl and Dr. Ming-Kuo Lee for their insight and contributions to this project. Their support during this process proved to be extremely beneficial and I am ever so grateful. I would like to thank Dr. Richard Blakely for his help and guidance with the modeling process. He is truly a master of his craft and his assistance gave me the assurance that I needed to confidently present my results.

I cannot thank my family and friends enough for their encouragement, support, and sacrifices they have given me throughout my life. I would not be the person I am today without each and every one of them. Most of all I'd like to thank my fellow graduate students that have endured this journey with me, side by side. The friendships that I have made during my time as a graduate student will last a lifetime. No matter how tough and challenging it became, I'll always look back at the fun we had together. It sure has been a fun ride.

# Table of Contents

# List of Tables

# List of Figures

# List of Abbreviations

| | |
|---|---|
| CBA | Complete Bouguer anomaly |
| CR | Modeled Crescent Formation |
| CRVP | Coastal Range Volcanic Province |
| GPS | Global positioning system |
| GRF | Green River fault |
| $G_{1-3}$ | Modeled quaternary glacial and post-glacial units |
| mGal | Miligal |
| nT | Nanotesla |
| $PG_{1-2}$ | Modeled Puget Group units |
| Qa | Quaternary alluvium |
| Qgd | Quaternary glacial deposits |
| QS | Quaternary glacial sediments |
| Qvt | Quaternary volcanic sediments |
| TFA | Total field anomaly |
| Tvt | Tertiary volcanic sediments |
| USGS | United States Geological Survey |
| WRF | White River fault |

# 1. INTRODUCTION

The Pacific Northwest (northern California, Oregon, Washington, and British Columbia) is widely known for its active tectonism and magmatism. This region, known as the Cascadia convergent margin, results from the oblique subduction of the Juan de Fuca plate beneath North America (Figure 1) (Blakely et al., 2011). Geodetic models suggest that this oblique motion is responsible for clockwise rotation (1°/Ma) and north-south compression as Washington collides with a slower-moving Canadian buttress (Blakely et al., 2011; Wells et al., 1998; McCaffery et al., 2013). Networks of faults and folds form in the northern extents of the Cascadian forearc in response to variable distribution of the regional north-south strain (Mazzotti et al., 2002; McCaffrey et al., 2013) (Figure 2). Recent studies have shown Holocene earthquakes, estimated to be a magnitude 7 or greater, have occurred along these faults (Bucknam et al., 1992; Kelsey et al., 2012). Thus, understanding the size, structure and location of active faults is key to assessing the area's earthquake potential.

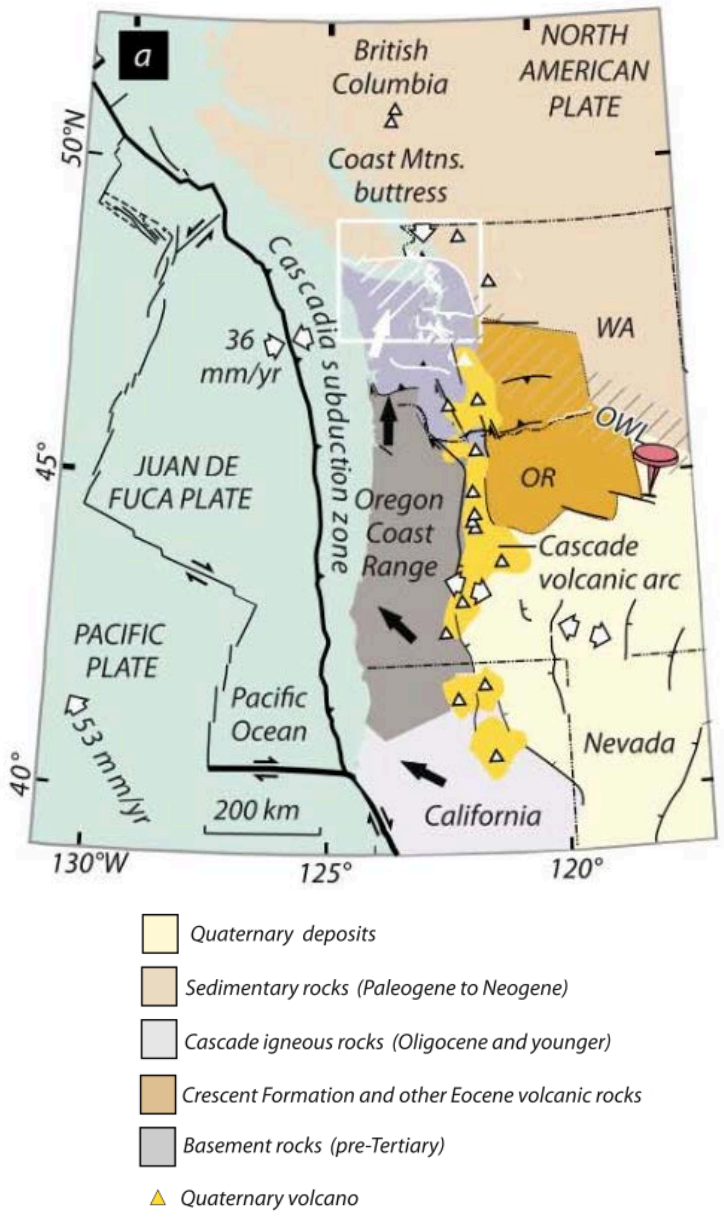


Figure 1. Regional tectonic map of Cascadia forearc system (modified from Sherrod et al., 2008)

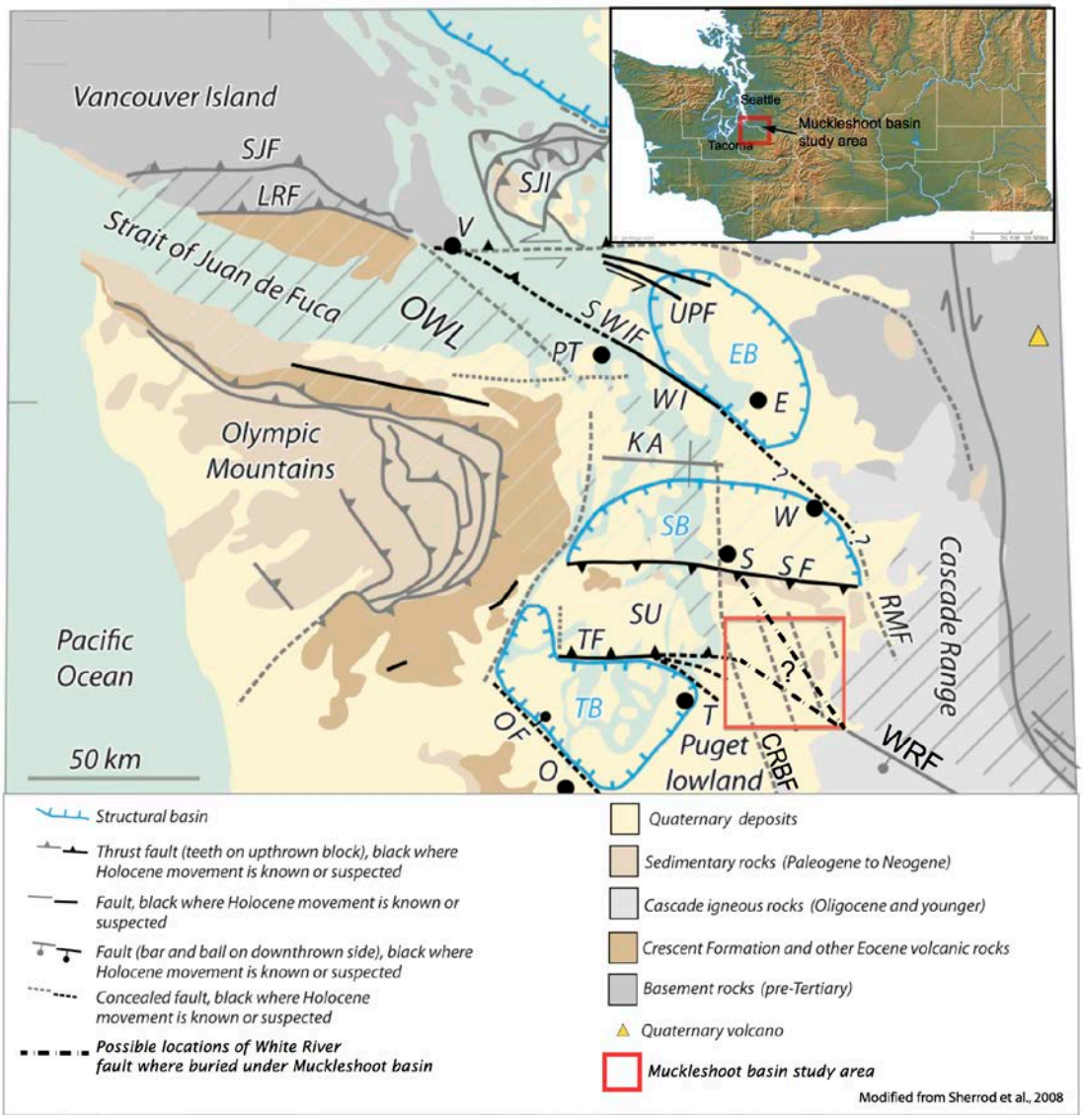


Figure 2. Generalized tectonic map of the Puget Lowland and surrounding regions modified from Sherrod et al. (2008). The Muckleshoot basin study area is shown with a red box. Structures of interest to this study are SB=Seattle basin, SU=Seattle uplift, TB= Tacoma basin, SF=Seattle fault, TF=Tacoma fault, WRF=White River fault, CRBF=Coast Range boundary fault, OWL=Olympic-Wallowa lineation, S=Seattle, T=Tacoma. Other abbreviations defined in Sherrod et al. (2008).

This project constrains the location and geometry of the faults in the Muckleshoot basin, which lies within the Puget Sound Lowland in the Pacific Northwest. Recent gravity and magnetic studies of the basin suggest that the White River fault, an active, steeply dipping thrust fault, mapped on the western margin of the Muckleshoot basin, may connect to other major active faults in the Puget Sound region (Figure 2) (Blakely et al. 2011; Taylor, 2013). The results of those studies, however, were inconclusive on whether the White River fault is connected with any of the major faults to the east of the basin. Such a connection would have significant implications for hazard estimates in terms of the length and size of these seismogenic structures and the maximum magnitudes that could be generated by faulting. Typical of the forearc basins within the Cascadia forearc, rock units beneath the Muckleshoot basin that could potentially contain evidence of fracture and folding are buried under younger sediments. In addition, Pleistocene-aged glacial deposits, as well as dense vegetation blanket surficial features making it essential to employ different methods to evaluate those structures.

This project (1) improves structural and geophysical models of the Muckleshoot basin and its relation to faults mapped outside the basin (Tacoma fault, White River fault, and Seattle fault), and (2) explores the depositional history of the Muckleshoot basin and how it relates to fault geometry and movement. This project's results have significance for estimating seismic hazard by helping to constrain geologic models of fault configurations near the highly populated Tacoma-Seattle area and provide insight on future tectonic models of strain accommodation in the Cascadia subduction zone and active margin.

# 2. GEOLOGIC BACKGROUND

## Muckleshoot basin

The Muckleshoot basin is located south of Seattle and east of Tacoma (Figure 2). It extends from the Puget Lowlands, near the city of Tacoma, to the foothills of the Cascade Mountains. It was described by vanWagoner et al. (2002) as being 7 to 9 km deep based on seismic and tomography data. Although there are no faults and folds that are exposed in the sedimentary basin, recent geophysical studies suggest the possibility of structures located beneath it. Any basement deformation could easily be hidden by thick deposits of Pleistocene and younger sediments that cover the basin.

The stratigraphy of Muckleshoot basin can be described generally as consisting of 6 separate units (Table 1)(Figure 3). In west-central Washington, east of the Olympic Mountains, the Crescent Formation forms the basement below the Puget Lowland. The entire Pacific Northwest is underlain by numerous large, Paleocene to late Eocene aged, volcanic extrusions known as the Coast Range volcanic province (CRVP). The Crescent Formation consists of marine basaltic rocks, interbedded with sedimentary rocks at the top of the formation. Overlying the Crescent Formation is the Late Eocene to early Oligocene Puget Group Formation. The Puget Group is subdivided into two units, differing by sediment type. The upper Puget Group sediments are mostly volcanic in origin whereas the lower Puget Group is composed of non-marine sedimentary rocks. The Ohanapecosh Formation is exposed on the eastern margin of the basin, overlying the Puget Group and consists of Oligocene volcaniclastics and flood basalts. The glacial and post-glacial strata represent the youngest layer in the basin. The glacial and post-glacial strata consist of clay, silt, and sand derived from rivers and Pleistocene glacial deposits.

The glacial and post-glacial strata vary in properties and are subdivided into three units for this study. The basal glacial unit is sand, pebbles and cobbles derived from interglacial and Pliocene deposits and is higher in density values than the upper two post-glacial sediments.

Table 1. Stratigraphy of the Muckleshoot Basin (Johnson et al., 2004; Finn, 1991)

| Unit | | Period | Time Interval | Tectonic Setting | Protolith |
|---|---|---|---|---|---|
| Glacial and Post Glacial Strata | 1 | Quaternary | Pleistocene - Holocene | Sedimentary basin, fluvial | Post-glacial clay, silt and sand derived from rivers and erosion of Pleistocene glacial deposits. |
| | 2 | | Pleistocene - Holocene | Sedimentary basin, fluvial, glaciation | Vashon Drift glacial and interglacial deposits (till, silt, sand and terrace gravel and stratified drift) |
| | 3 | | | | |
| Ohanapecosh Formation | | Paleogene | Oligocene | Flood basalts | Volcaniclastic deposits and flood basalts |
| Puget Group | 1 | | Eocene | Non-marine to marginal marine | Intertongued volcanics and non-marine to marginal marine sedimentary rocks. |
| | 2 | | Eocene | | |
| Crescent Formation | | | Eocene | Marine | Marine basaltic rocks that form the basement in the study area. Tend to be dense and magnetic. Interbedded basalt and sedimentary rocks at top of formation. |

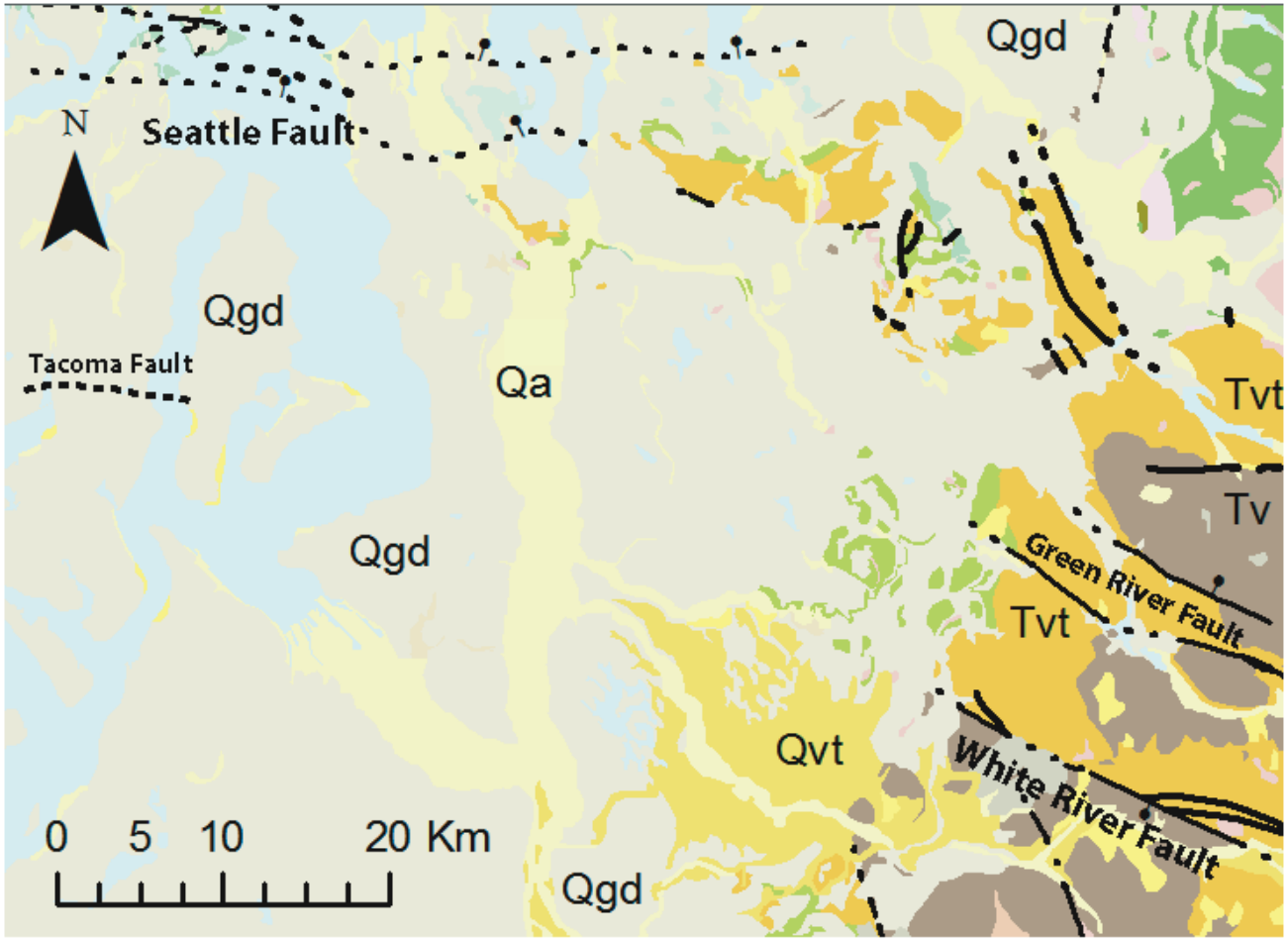


Figure 3. Surficial geologic map of Muckleshoot basin. Geologic map modified from Washington DNR (2013).

## Basin Depositional History

The Crescent Formation is the most voluminous of the Coast Range volcanic sequence and is known to be as much as 16 km thick (Babcock et al., 1992). It is composed of predominantly pillowed to massive flows and flow breccias, massive coarse-grained sills or sheet-flows interspersed throughout. The upper portion of the Crescent Formation is interbedded with sedimentary units such as sandstone, siltstone and conglomerate (Babcock et al., 1992). Initial interpretations of the CRVP were documented as an accreted seamount chain extruded on an oceanic plate. Although the origin of the Crescent volcanics is still uncertain, recent evidence has shown that the massive extrusions were a result of rifting in the forearc during plate subduction about 60 Ma (Babcock et al., 1992).

Overlying the volcanic basement Crescent Formation lays the non-marine to marginal marine, Eocene aged, Puget Group. The Puget Group is a thick sequence of arkosic and volcanic rocks that outcrop throughout most of west-central Washington (Buckovic, 1979). The thickness of the Puget sequence in west-central Washington exceeds 2700 m and is divisible into formational units were marine and volcanic units are present. The majority of the Puget Group in the Puget Lowland consists of an extensive facies of nonmarine sandstone, siltstone, mudstone and coal (Figure 4 and 5). In some areas, although much less exposed, the Puget Group consists of marginal marine and marine facies of alternating sandstone, siltstone, mudstone and coal sequences interpreted as channel deposits of a delta plain facies (Buckovic, 1979) (Figures 4 and 5).

Figure 4. Photograph of Puget Group exposure along the White River.

Figure 5. Photograph of outcropping sandstone of the Puget Group sequence.

The Puget deltaic system formed as the result of rapid basin subsidence and high rates of sedimentation along a low-energy marine interface. The Puget Delta was a bird-foot complex system similar to the modern day Mississippi delta. Most of the delta's sediments, comprised of arkosic material, derived from a granitic source terrain of moderate relief (>1200 m), and were transported across a broad, low lying continental platform to the delta (Buckovic, 1979). Simultaneously, during the Eocene, a westward shift of plate subduction caused a widespread volcanism increase in the Pacific Northwest. The increase in volcanism appears to have had no affect on the mode and rate of deposition in the delta, however, the significant changes to the distribution and thicknesses of the Puget sequence did occur. Within the Puget Group, volcanic sediment sequences are intertongued which resulted in the Puget Group being modeled into two units slightly varying in density and magnetic susceptibility. In the early Oligocene, volcanic sediments derived from a major volcanic high east of the Puget delta buried the Puget Deltaic systems in west-central Washington (Buckovic, 1979).

Repeated Pleistocene glaciation in the Puget Lowland is apparent due to the interbedding of glacial drift and nonglacial deposits mapped in the area (Figure 6). These glacial and interglacial deposits indicate that the area was glaciated at least 6 times during the Pleistocene (Mullineaux, 1970). These deposits are roughly 400 m thick in the southern Puget Lowland, near Tacoma. The most recent glacial advance in the Puget Lowland was the Puget lobe of the Cordilleran Ice Sheet, a continental glacier that originated in British Columbia (Figure **7**). Culminating ~15,000 B.P., the Puget lobe moved southward from British Columbia into and across the Puget Lowland. The drift sheets associated with the Puget lobe are recognized as having a northern origin because of the rocks and minerals they contain. Most of these rocks

found in these drift sheets are typical of the mountains of British Columbia and northern Washington, and are not native to the Cascade Range drained by rivers that flow into the Puget Lowland (Mullineaux, 1970).

Figure 6. Photograph of semi-cemented rounded cobbles and pebbles typical of a Glacial till deposit within the Muckleshoot basin.

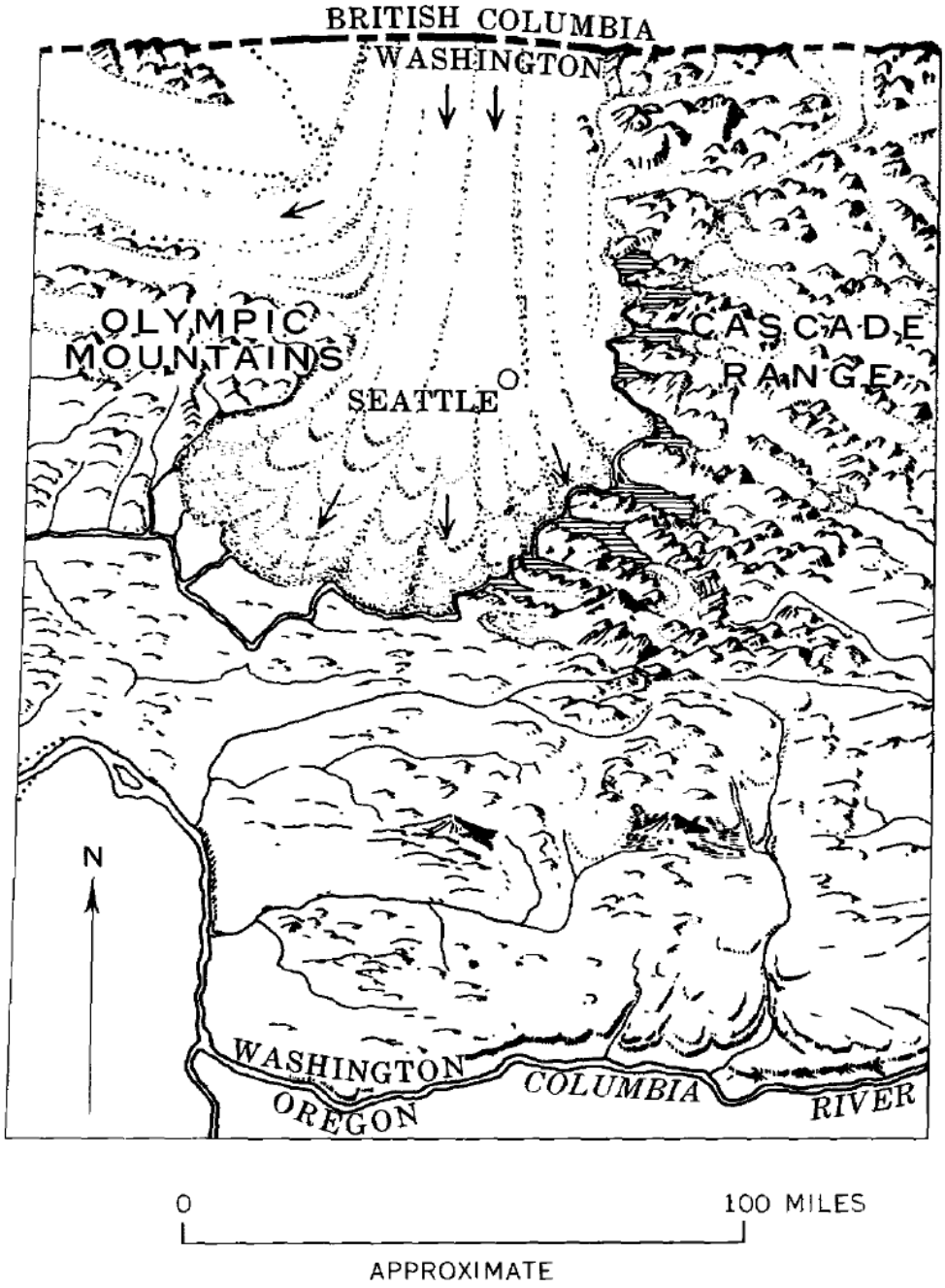


Figure 7. Illustration of Puget Lobe of the Cordilleran Ice Sheet encroaching from British Columbia (Mullineaux, 1970)

### Active Faults of the Puget Lowland

A system of east west and northwest striking crustal faults cross the Puget Lowland accommodating the compression caused by the collision with the slower moving Canada buttress (Wells et al., 1998). Most of the faults have shown activity within the Holocene and are associated with the structural basins and uplifts seen in gravity, magnetic and seismic data (Blakely et al., 2011). Four Holocene faults within the study area are of great importance to this study: the Seattle fault zone, Tacoma fault, White River fault and Green River fault (Figure 3).

The Seattle fault zone consists of multiple east-trending, north-verging thrust faults. Motion on the fault zone has displaced Eocene volcanic and sedimentary bedrock northward relative to the deep, sediment-filled Seattle basin to the north (Johnson et al., 1994; Blakely et al., 2002). Johnson et al. (1994) postulated that the Seattle fault zone has been active from 40 Ma to the present and represents an east-trending compressional zone that transfers strain from right-lateral faults located southeast and northwest of the Seattle fault zone.

The Tacoma fault is an active south-verging reverse fault that extends from the western edge of the Muckleshoot basin westward beneath the waters of the Puget Sound (Blakely et al., 2007). The Tacoma fault controls the boundary between the Tacoma basin to the south and the Seattle uplift to the north. However, gravity data and seismic tomography do not show strong evidence to suggest the Tacoma basin extends more than a few km east of Puget Sound (e.g. Pratt et al., 1997; Brocher et al., 2001; VanWagoner et al., 2002; Johnson et al., 2004). Aeromagnetic data show a west-northwest trending lineament that appears to follow the Tacoma fault; however, this anomaly continues eastward into the Muckleshoot basin, where both the White River fault and Tacoma fault disappear (Blakely et al., 2007) (Figure 3).

In 2007, Liberty et al. collected new land-based seismic data along the eastern margin of the Muckleshoot basin. He and his team integrated the new reflection data with seismic tomography, gravity and magnetic data to characterize the basin subsurface and locate any faults associated with the Tacoma fault zone (Figure 8 and 9). Their study showed evidence of both north-south and east-west shortening of the basin as well as a segmentation dividing the basin into two sub-basins. However, no structures or faults associated with the Tacoma fault zone were identified.

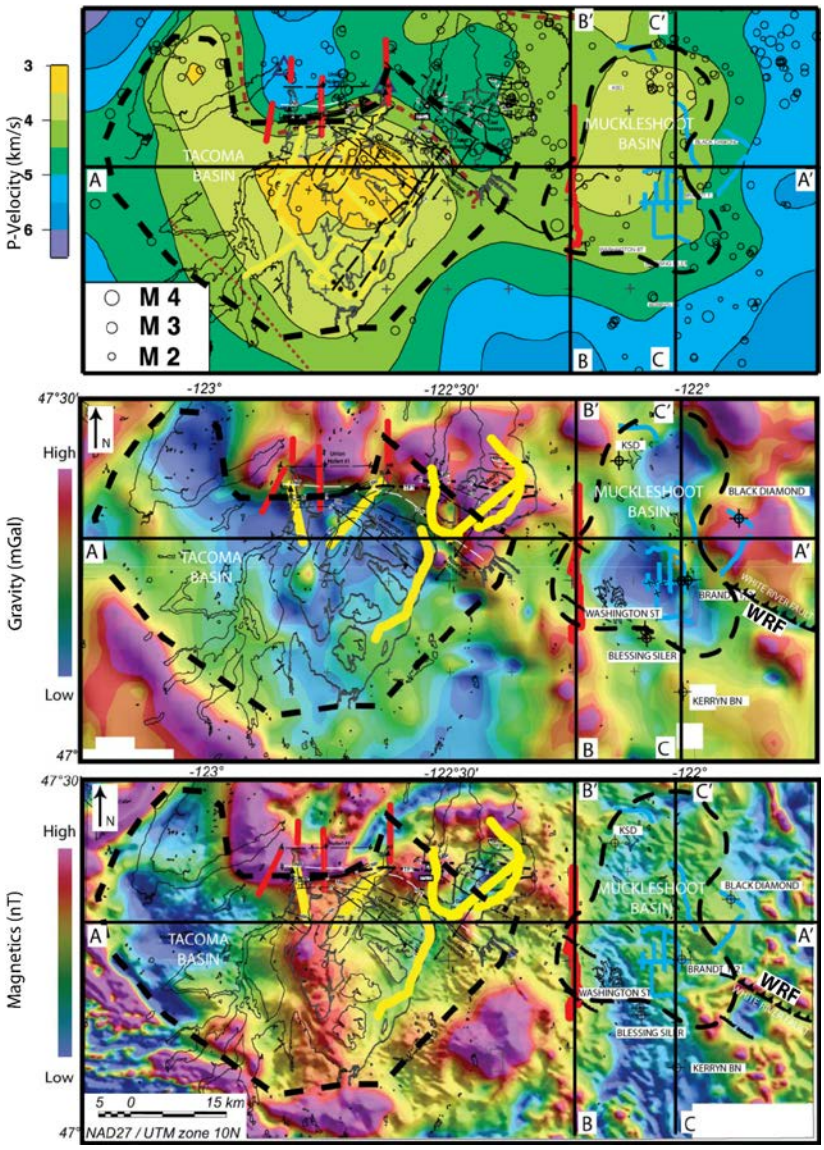


Figure 8. Seismic tomographic image (top) from 2.5 km depth, isostatic residual gravity map (middle), and magnetic anomaly map (bottom) for the Tacoma and Muckleshoot basins (Liberty, 2007). Red lines are high-resolution land-based seismic reflection profiles. Lines A-A′, B-B′, and C-C′ coincide with profiles in Figure 4. WRF= White River fault. Basins are outlined with dashed black lines. Other lines represent features as listed in Liberty (2007).

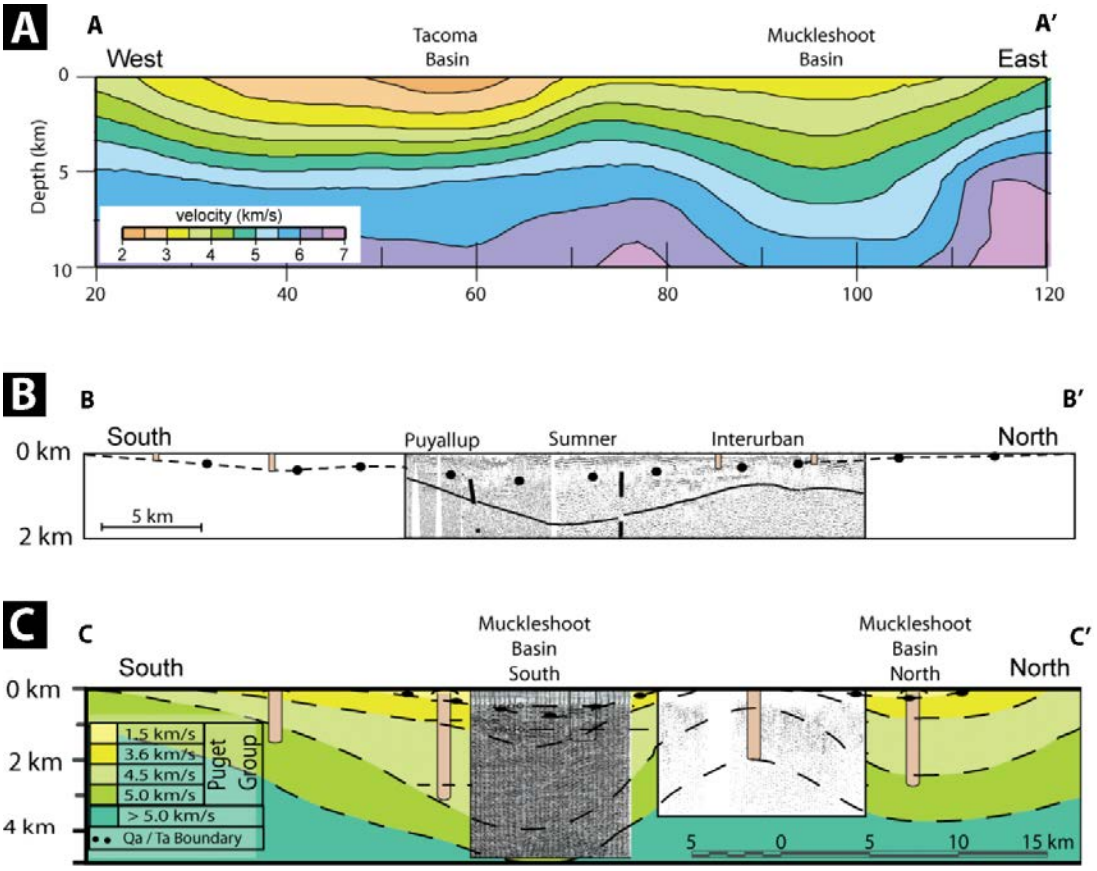


Figure 9. Cross-sections of the Muckleshoot basin from profiles in Figure 8 (Liberty, 2007). (a) A-A′ is a west to east tomographic cross-section; (b) B-B′ is a south to north cross-section that shows seismic data, borehole data, and estimated Quaternary strata depth; (c) C-C′ is a south to north cross-section that combines seismic data, borehole data, and velocity data. Light brown vertical bars are wells used to constrain lithology in Liberty's study.

The west-northwest trending White River fault was interpreted by Tabor et al. (2000) as a steep, south-dipping normal fault. More recent work suggests that it is a steep reverse fault dipping to the south (Box et al., 2003). The White River fault can be traced from east of the Cascade Range to the Puget Lowland, where it juxtaposes the early Miocene Fifes Peak Formation against the Oligocene Ohanapecosh Formation (Figure 9) (Tabor et al. 2000). Gravity data of the Muckleshoot basin show a basement high that appears to line up with the projection of the White River fault into the basin (Liberty, 2007; Blakely et al., 2011).

Blakely et al. (2011) and Reidel and Campbell (1989) argue that based on magnetic anomalies, the WRF appears to cut through the Cascade Mountains and merge with the Umtanum Ridge fault northeast of Cleman Mountain, north of Naches, Washington. If the Tacoma fault merges with the WRF beneath the Muckleshoot basin, the WRF Zone extends from just east of the Olympic Mountains to Umtanum Ridge, totaling over 185km (Blakely et al., 2011).

The Green River fault is located just north of the WRF and is interpreted to be a similar steep, south-dipping reverse fault (Blakely et al., 2011). The fault follows along the Green River eastward into the Cascade Mountains and westward into the Muckleshoot basin. Like the WRF, the Green River fault is unable to be traced on the surface within the study area due to the quaternary cover of the Puget Lowland.

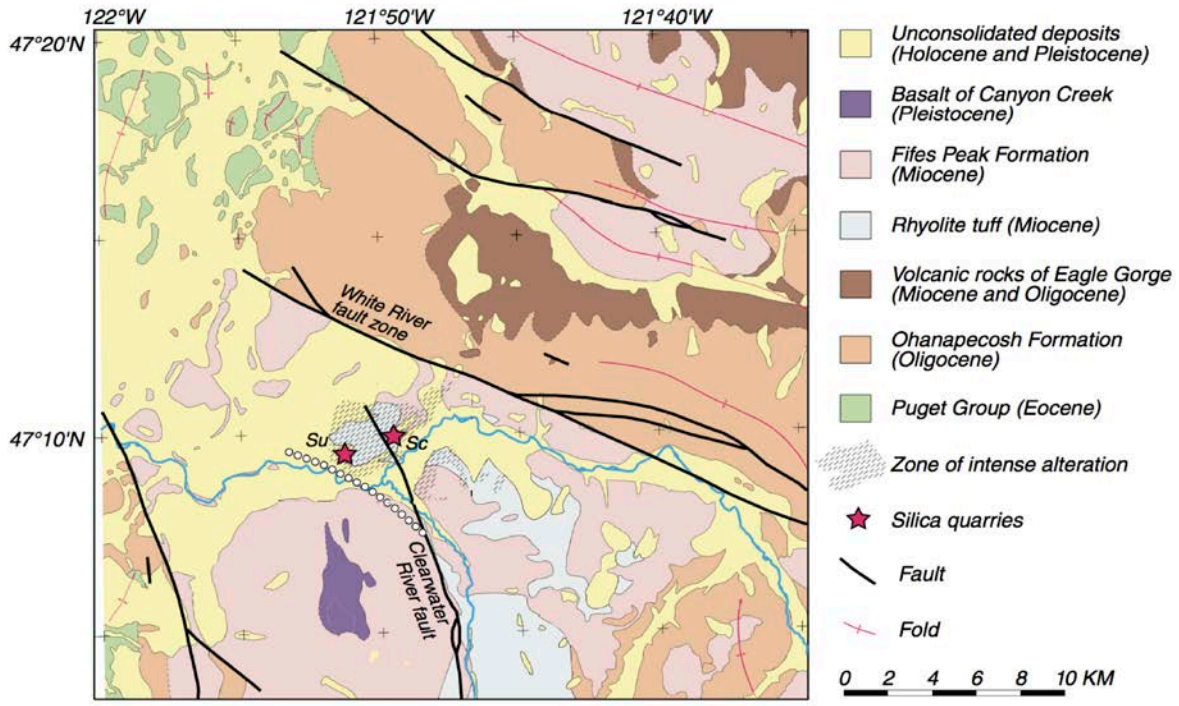


Figure 10. Geologic map showing juxtaposition of bedrock units separated by White River fault zone. White dotted line is splay of Clearwater River fault discussed in Blakely et al., 2007. Modified from Blakely et al. (2007).

# 3. METHODOLOGY

## Gravity and Magnetic Data Collection

New gravity data used in this study was collected within the Muckleshoot basin study area and were merged into the area's existing gravity database (Dater, 1999; Taylor, 2013) (Figure 11). Refer to Taylor (2013) for further details about the acquisition and mergence of gravity data.

The Magnetic data used in this study were acquired from the USGS in spreadsheet form that contained total field anomaly (TFA) values and location coordinates for each measurement (Blakely et al., 1995). Once the magnetic data was acquired, it was reduced to pole to recalculate the data as if the inducing magnetic field had a 90° inclination. This makes the assumption that the rocks units in the study area are all magnetized parallel to the earth's magnetic field.

## Magnetic Susceptibility Data

Several exposed outcrops of the upper Puget Group were located on geologic maps prior to field reconnaissance that would allow magnetic susceptibility readings to be easily obtained. Measurements were taken on exposed surfaces of the targeted geologic units, then recorded and documented. Magnetic susceptibilities of exposed geologic units were measured using a Terraplus KT-10 v2 Magnetic Susceptibility/Conductivity Meter to improve curve matching during the modeling process and provide realistic estimates for specific formations.

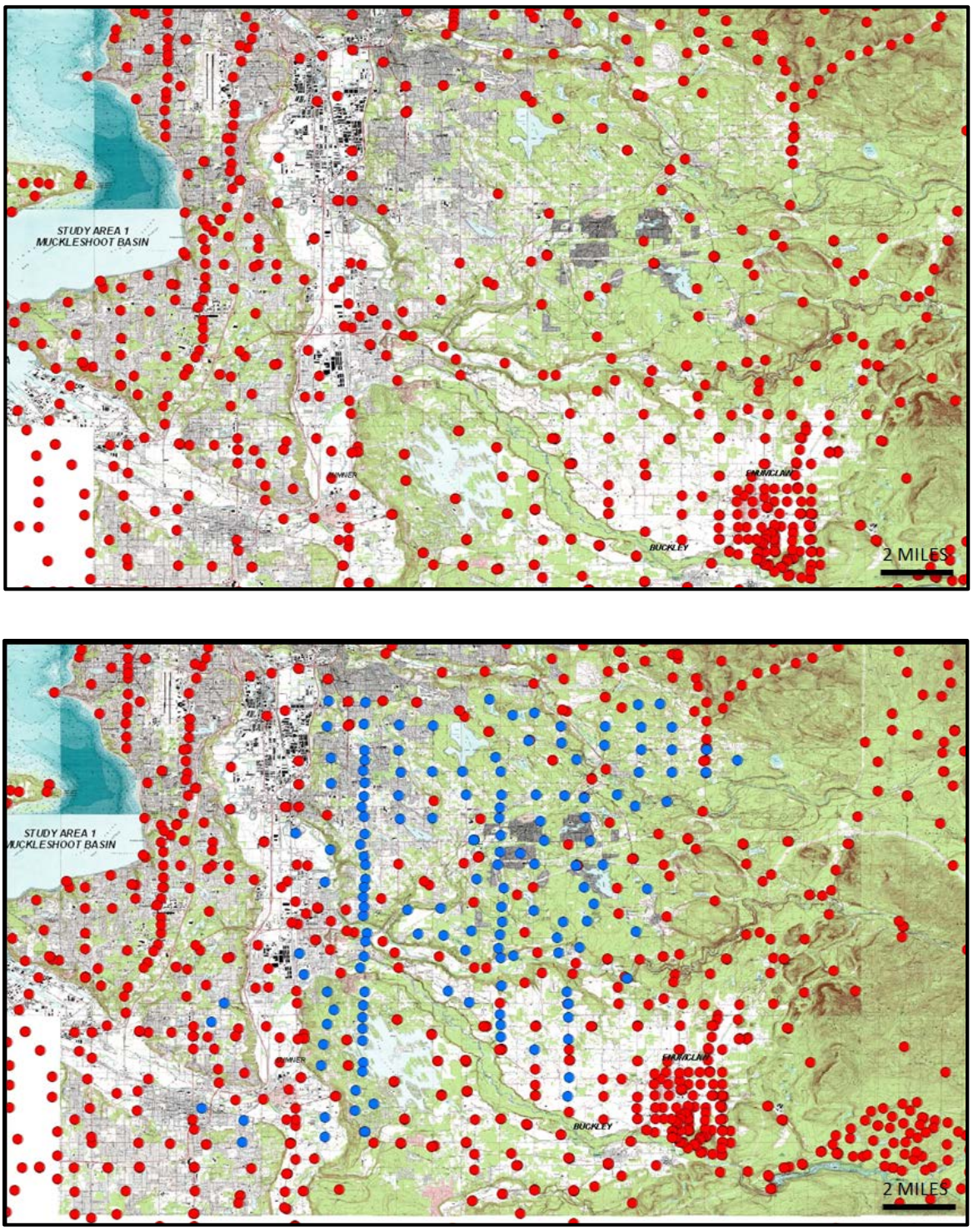


Figure 11. Locations of gravity sites/stations in the Muckleshoot study area. The top map shows the existing measurements before fieldwork began (red dots) superimposed on an area made up of 15 (1:24000) USGS topographic maps. The bottom map shows both the existing locations and new locations (blue dots) acquired during fieldwork in Taylor, (2013).

## Ancillary Data

In addition to gravity and magnetic data, other supporting data, such as well-log data, geologic maps, and field measured magnetic susceptibilities of exposed rock types were compiled for the current study. Well-log data were used to constrain the lithologies of the upper few kilometers, and seismic data were used to constrain the deeper crust. Geologic maps were utilized to locate major geological boundaries along the modeled profile lines. Physical properties of the subsurface rocks were used to produce the gravity and magnetic starting models.

## Data Processing

Gravity and magnetic data were gathered and organized separately in preparation for modeling. Geosoft's Oasis Montaj™ software was used for processing the data. This software offers many tools for data manipulation, including data reduction, filtering, mapping, and gridding. Oasis Montaj™ is designed to work with Geosoft's GM-SYS® profile modeling software. GM-SYS® assists in building and constraining two-dimensional models at depth. The program uses variables such as depth, thickness, density, and susceptibility to define rock units and structures. It is crucial to reduce the gravity anomaly map to a common datum so that Bouguer anomalies can be more confidently interpreted to reveal subsurface bodies of exploration interest. All data gravity data within this study were corrected using standard methods and calculated with a reduction density of 2.67 g/cm$^3$.

## Data Modeling

Gravity and magnetic cross-sectional models were constructed along three transects (A-A′, B-B′, and C-C′) from the regional data set and crustal models were built along those transects (Figures 12). Locations of these transects were chosen so that they cross parallel to the potential field gradient to minimize three-dimensional effects. The location of each transect was specifically placed to target the White River Fault, Tacoma Fault, and other features of interest.

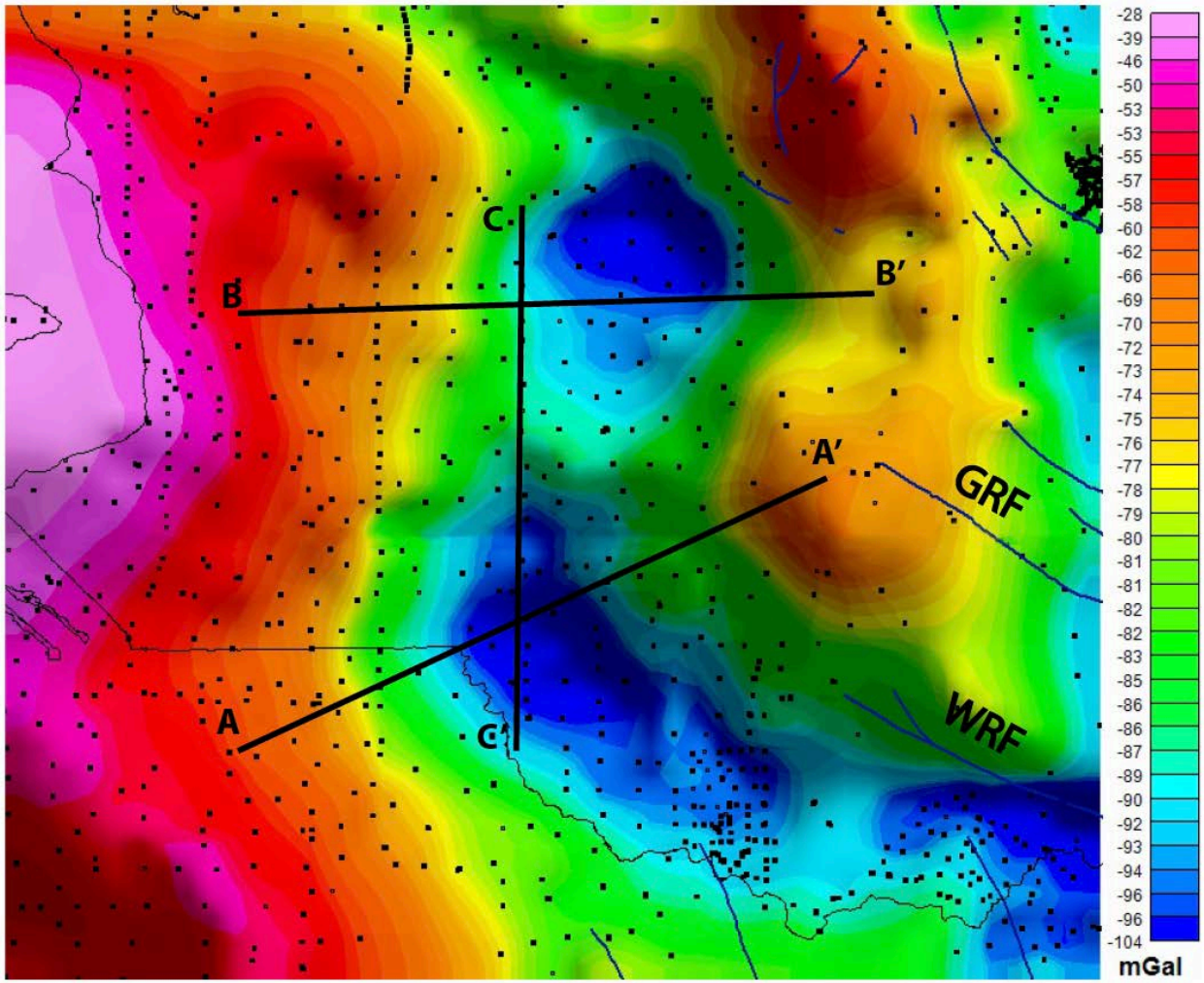


Figure 12 Gravity (CBA) map of the Muckleshoot study area with profile locations. Solid blue lines=faults. Abbreviations: WRF=White River fault, GRF=Green River fault.

Crustal models along the three transects were developed using Geosoft's Oasis Montaj and GM-SYS software. The GM-SYS software calculates both gravity and the magnetic values for a geologic model. Forward modeling, which was used for this study, provides an option for joint inversion of the gravity and the magnetic data. Two-dimensional modeling only considers the gravity effect produced by the bodies directly below the line, whereas Oasis Montaj's 2.5 dimensional modeling expands the theoretical calculation to include the effects of the bodies perpendicular to the line.

Rock units or layers in the model are represented by polygons. Each layer was assigned density and susceptibility properties based on the major rock types assumed to be present. The ranges of density and magnetic susceptibility values can be found in Table 2. Initial models assumed simple parallel boundaries, which were then modified by incorporating information from published geologic cross-sections, seismic data interpretations (if available), and seismic velocity profiles. Once the basic geologic cross-section had been constructed and properties were entered, polygons were manipulated to adjust the calculated gravity and magnetic curves until a satisfactory match to the data was achieved. Geologic features, such as faults, were added to the model to compensate for strong dips in the observed magnetic curve signature.

Table 2 Block symbols, densities, magnetic susceptibilities and lithologies listed for each subsurface unit (Johnson et al. 2004; Babcock et al. 1992; Buckovic, 1979; Mullineaux, 1970).

| Body symbol | Unit name | Modeled rock density ($g/cm^3$) | Modeled rock susceptibility (SI) | Rock description |
|---|---|---|---|---|
| G1 | Glacial and Post Glacial Strata | 1.8-2.0 | 0.00001-0.00003 | Clay, silt, and sand derived from rivers and erosion of Pleistocene deposits. |
| G2 | | 1.9-2.0 | 0.00001-0.00004 | Clay, silt, and sand derived from rivers and erosion of Pleistocene deposits. transitional and interglacial deposits |
| G3 | | 2.0-2.2 | 0.00002-0.00007 | |
| P1 | Puget Group | 2.2-2.6 | 0.00007-0.0002 | Volcanoclastic deposits and flood basalts |
| P2 | | 2.6-2.8 | 0.00007-0.0002 | Volcanics and non-marine sedimentary rocks. |
| Cr | Cresent Formation | 3 | 0.00003 | Marine basaltic rocks that are dense and magnetic. Sedimentary rocks are inter-bedded at the top of the formation. |

# 4. RESULTS

## Muckleshoot Basin Gravity Maps

A complete Bouguer anomaly map was initially produced by combining all old and new measurements into a color shaded grid map (Figure 13). The CBA map is used to help identify broad feature of basin structure and extent. All observed CBA gravity values were calculated with a reduction density of 2.67 g/cm$^3$ and are shown as negative. Values range from -28 mGal (high) to -104 mGal (low). The lowest anomaly values are observed within the center of the study area and middle of the basin. This low coincides with the portion of the basin where the most amount of sediment has been deposited. There are gravity highs on both edges of the map and these are thought to mark the approximate outer extent of the basin sediments. A ridge-like gravity high trends northwest through the basin, segmenting the basin into two gravity lows.

## Muckleshoot Basin Magnetic Maps

Figure 14 contains a map of magnetic data showing the TFA. The lowest magnetic TFA values (-2316 nT) are observed in the south and east sections of the map. The highest TFA values (520 nT) are shown along the western edge and in several areas in the southeastern corner of the map. White rectangles in the southeast corner are artifacts caused by gaps in data coverage. Within the basin margins, there is a general trend of northwest-southeast striking anomalies. These anomalies are oriented along the same trajectory as the mapped WRF and GRF fault lineations. A large magnetic high on the western side of the map corresponds to a gravity high on the CBA map. This magnetic high denotes the western extent of the Muckleshoot basin. As in gravity anomaly maps, these sharp contrasting anomaly values are typical of thrust faults juxtaposing two units with different magnetic susceptibilities.

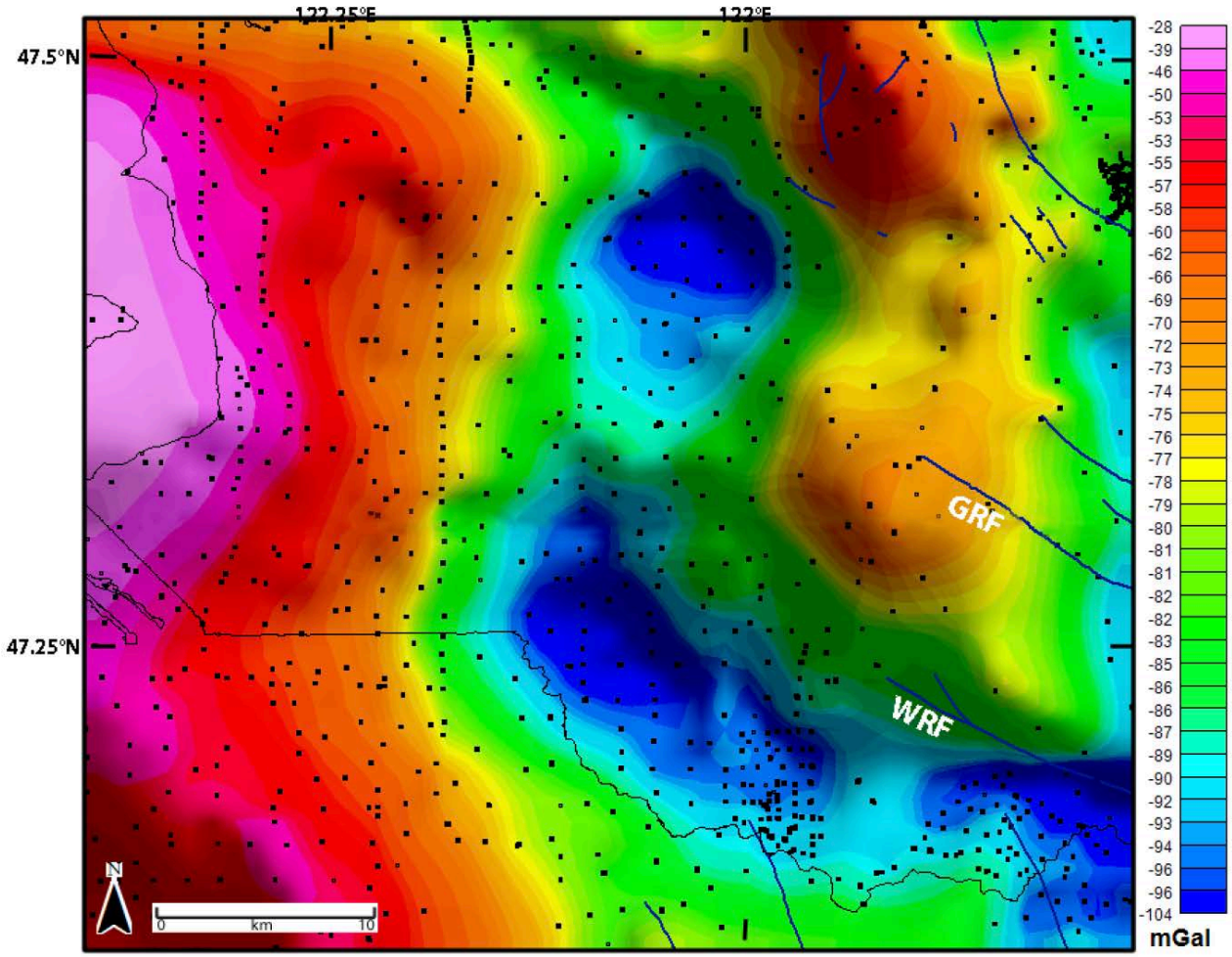


Figure 13. Gravity (CBA) map of the Muckleshoot study area. Black dots=station locations. Solid blue lines=faults. Abbreviations: WRF=White River fault, GRF=Green River fault

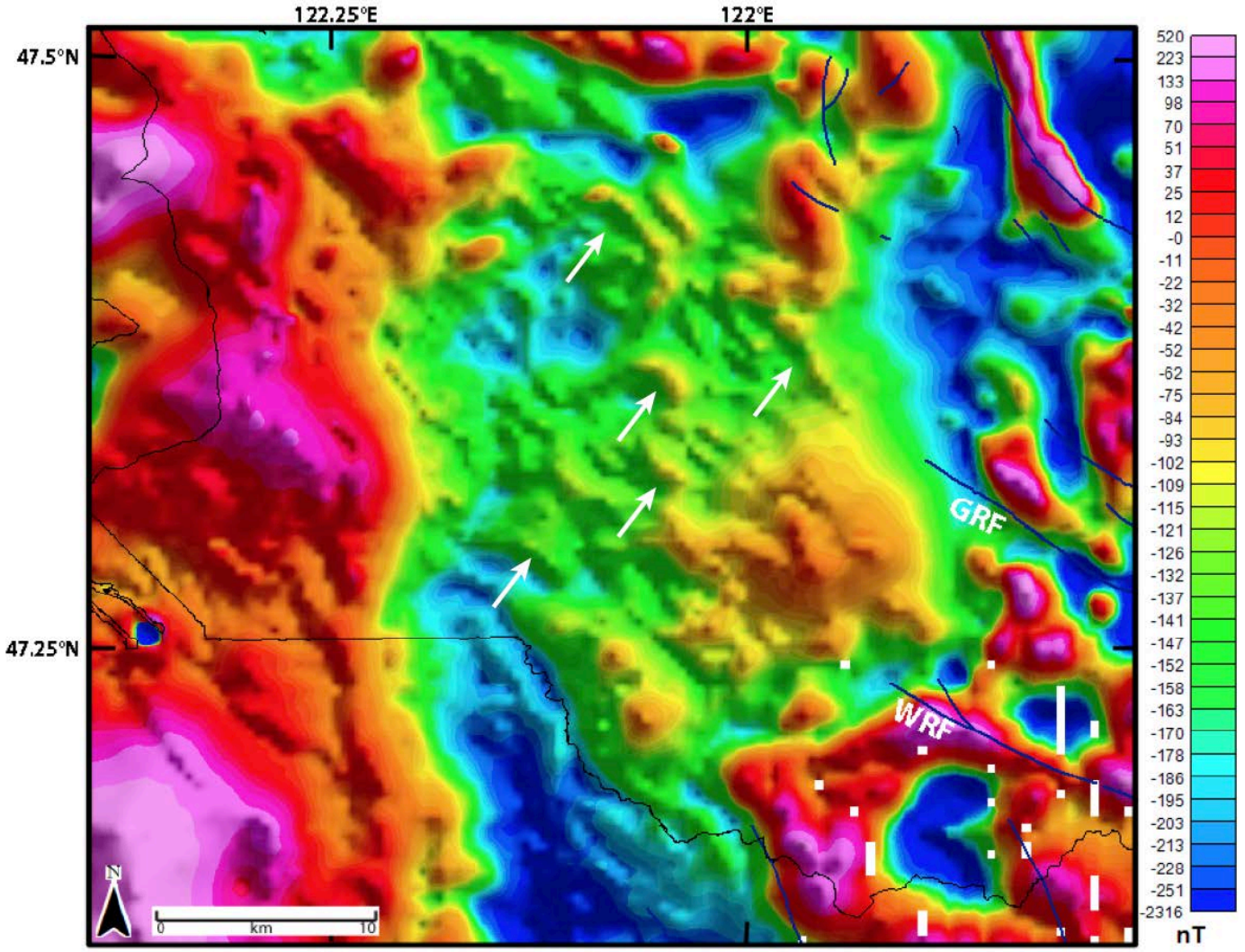


Figure 14. Magnetic (TFA) map of the Muckleshoot study area. White rectangles in the southeast corner are artifacts caused by gaps in data coverage. White arrows= Northwest-southeast trending anomalies. Solid blue lines=faults. Abbreviations: WRF=White River fault, GRF=Green River fault.

## Vertical Derivative Maps

A vertical derivative convolution filter was applied to both the gravity and magnetic maps to further highlight the locations of structures within the study area. A vertical derivative filter emphasizes boundaries with high gravity and magnetic gradients and in turn, accentuates features like fault contacts (Blakely et al., 2011; Grausch et al., 2013).

Values on the gravity derivative map range from -0.0150 mGal/km (low) to 0.0100 mGal/km (high) (Figure 15). Steep gradients often mark basin boundaries or two juxtaposed units with contrasting densities. This juxtaposition is often caused by a fault-induced offset (Graush et al., 2013; Blakely et al., 2011). A steep gradient appears in the northwest corner of this map possibly corresponding with the northern boundary of the Seattle uplift and the location of the Seattle fault zone. At the southeastern corner of the map a very steep gradient is visible likely coinciding with the location of the White River fault where it is juxtaposes the less dense Fifes Peak formation with the Ohanapecosh flood basalts. The typical gravity low associated with the Muckleshoot basin is very noticeable on the vertical derivative map. Within the gravity low basin, several gravity high "mounds" trending in a northwest-southeast direction. These small, but steep gradients align with the northwest trending gravity high ridge segmenting the basin seen in the CBA map (Figure 13).

A vertical derivative filter was applied to the TFA map to provide evidence of fault locations within the basin (Figure 16). Differences in data coverage cause the appearance of the same white anomalies along with slight rippling in the immediate surrounding areas. Values range from -9.4 nT/km (low) to 1.9 nT/km (high). The western margin of the Muckleshoot basin is outlined by a high gradient. Two strong magnetic gradient changes appear along strike with the mapped locations of the WRF and GRF. Sharp contrasts values (steep gradients) form linear features that align with previously mapped locations of the faults. A steep east-west trending gradient is noticed in the far northwest corner of the map, which aligns with the projection of the well-known Seattle fault zone. The eastern boundary of the Muckleshoot basin is defined by the contact of the Ohanapecosh Formation on the east with the quaternary sediments infilling the basin.

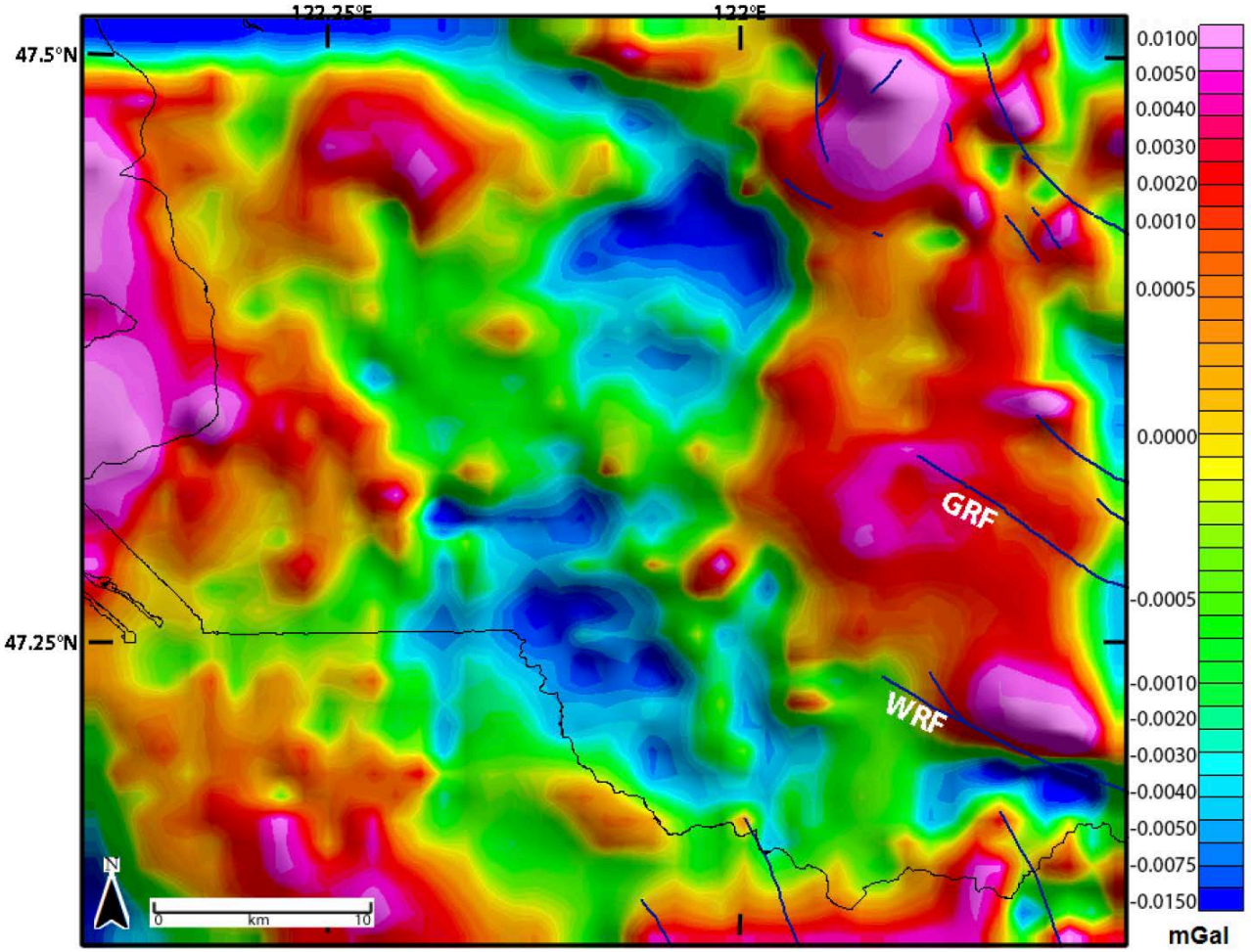


Figure 15. Gravity (CBA) map of the Muckleshoot study area with vertical derivative filter applied. Solid blue lines=faults. Abbreviations: WRF=White River fault, GRF=Green River fault

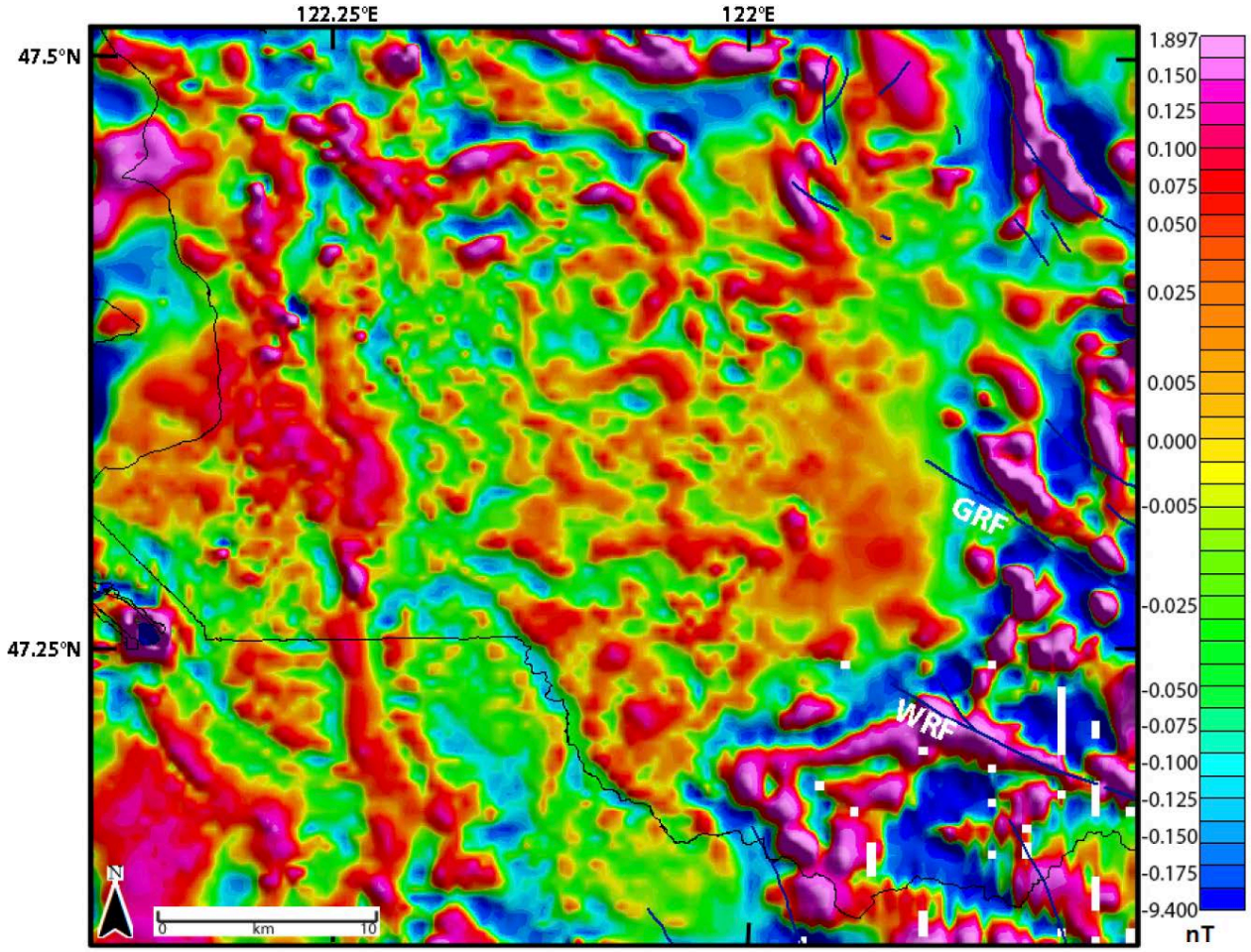


Figure 16. Magnetic (TFA) map of the Muckleshoot study area with vertical derivative filter applied. Solid blue lines=faults. Abbreviations: WRF=White River fault, GRF=Green River fault.

## Gravity and Magnetic Profiles

Three gravity and magnetic profiles (A-A′, B-B′, and C-C′) were constructed to model the subsurface of the Muckleshoot basin (Figure 17). Four factors were considered in choosing the profile locations: (1) the density of gravity and magnetic data coverage, (2) the magnetic and gravity gradient (profiles were positioned parallel to the gradient to minimize three-dimensional effects), (3the postulated locations of previously mapped faults on the basin margins, and (4) the need for a three-dimensional model constrained by intersecting profiles.

Line A-A′ is oriented northeast-southwest and crosses the gravity low associated with the Muckleshoot basin south of the gravity high segmentation seen on the CBA map. The entire length of the profile is 23.56 km and is positioned across the projected trace of the White River fault. Line B-B′ is oriented east-west and crosses the north of the gravity high that segments within the basin. Profile B-B′ is 25.66 km and was positioned to intersect the projected trend of the Green River fault into the basin. Profile C-C′ is oriented north-south crossing the Muckleshoot basin. The location of C-C′ was chosen to follow a dense transect of ground measurements and to provide a tie with the other two profiles. Profile C-C′ is 21.5 km and crosses the gravity high in the center of the basin. All three cross-sections extend 9 km below the surface. Surface contacts of rock units in and outside of the modeled cross-sections were used to constrain boundaries between polygons and the location of structures, such as faults and folds (Figure 16) (Washington State DGER, 2014).

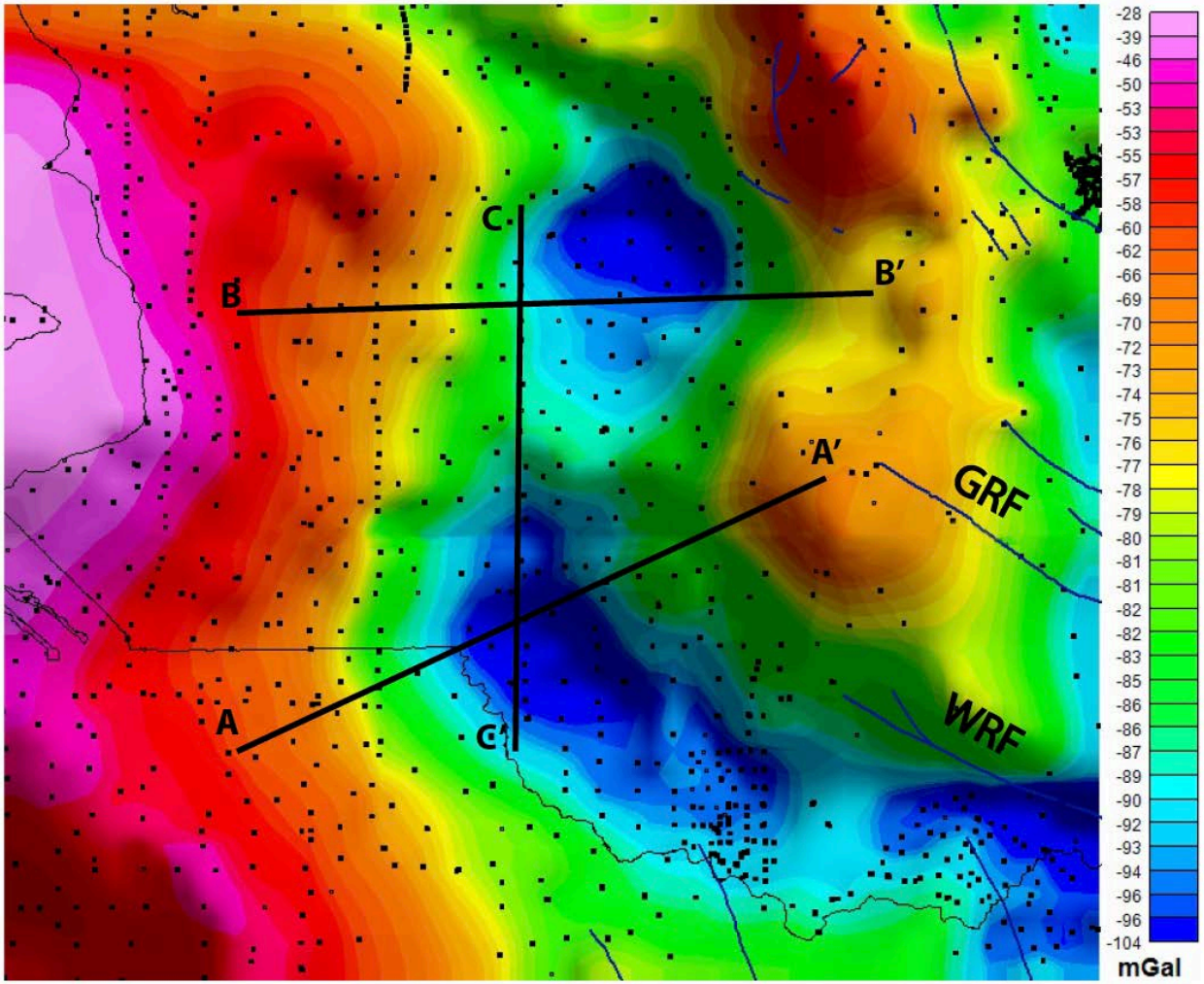


Figure 17. Gravity (CBA) map of the Muckleshoot study area with profile locations. Solid blue lines=faults. Abbreviations: WRF=White River fault, GRF=Green River fault.

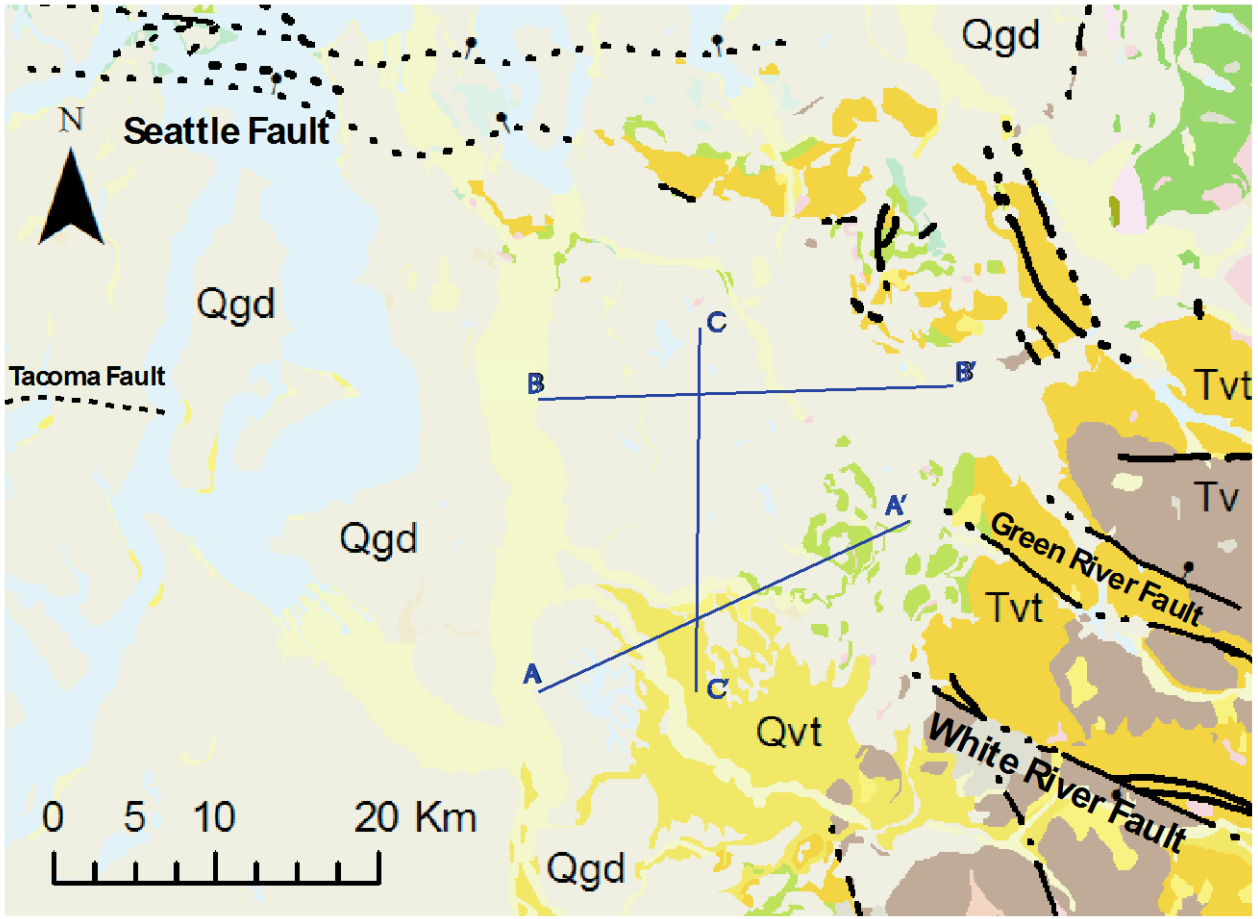


Figure 18. Surface geologic map of study area with profile locations. Qgd=quaternary glacial sediment. Qvt=Quaternary volcanic sediment. Tvt=Tertiary volcanic unit. Geologic map modified from Washington DNR (2013).

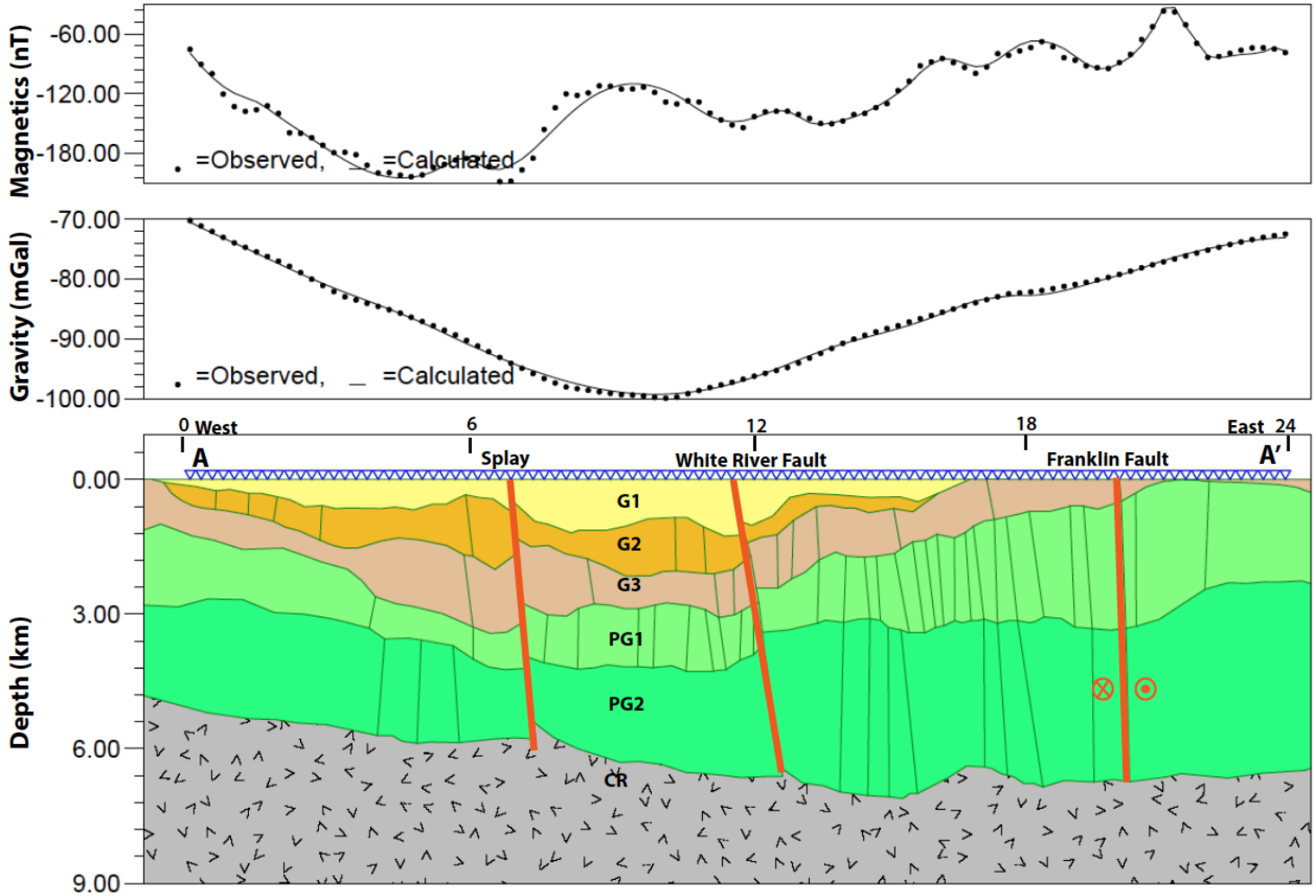


Figure 19. Gravity and magnetic profile A-A′. Abbreviations: G1=Glacial and post-glacial strata 1, G2=Glacial and post glacial strata 2, G3=Glacial and post glacial strata 3, P1= Puget Group 1, P2= Puget Group 2, CR= Crescent Formation, red lines = fault locations, red X= movement away from observer, red circle=movement towards observer.

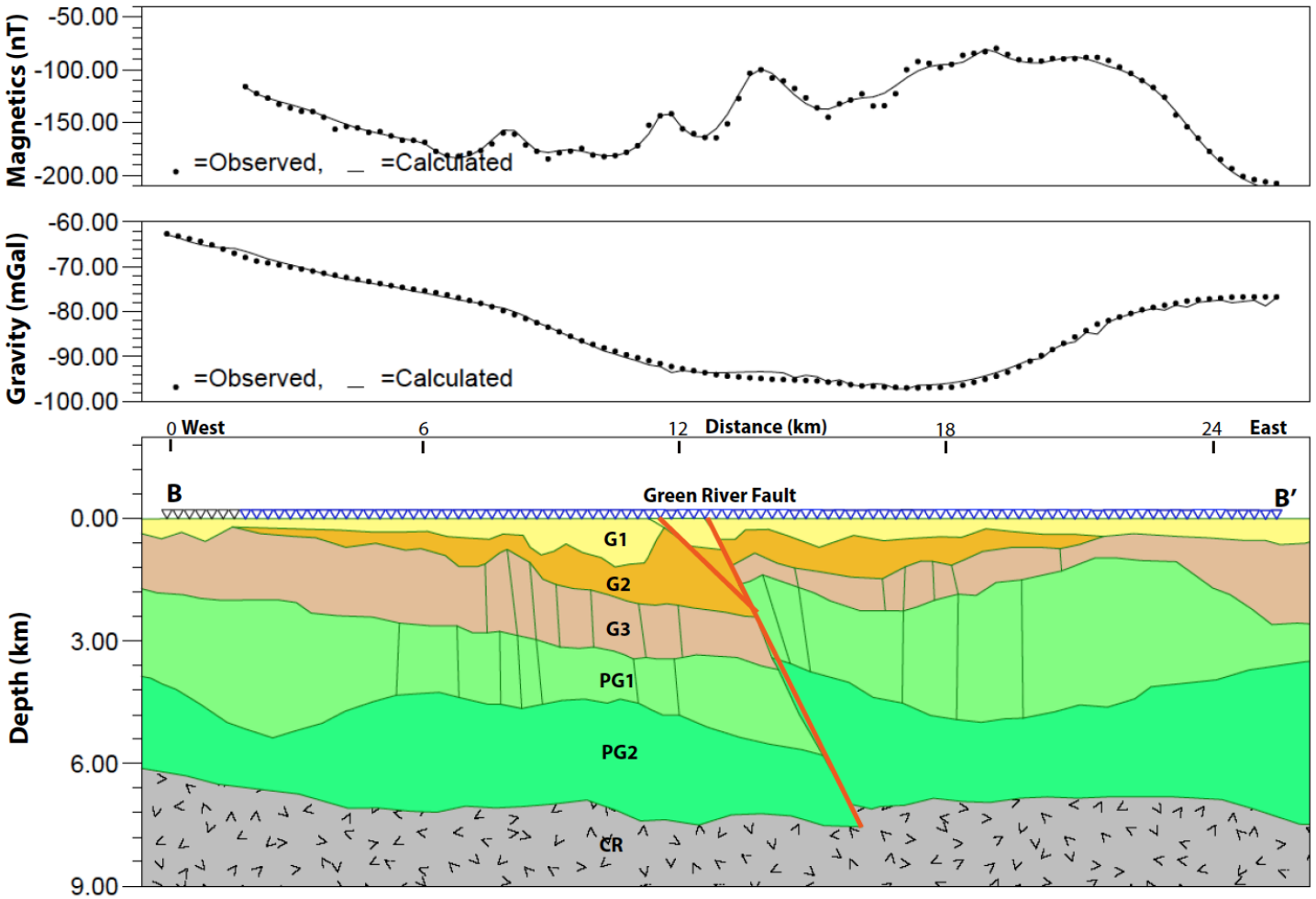


Figure 20. Gravity and magnetic profile B-B′. Abbreviations: G1=Glacial and post-glacial strata 1, G2=Glacial and post-glacial strata 2, G3=Glacial and post-glacial strata 3, P1= Puget Group 1, P2= Puget Group 2, CR= Crescent Formation, red lines=fault locations.

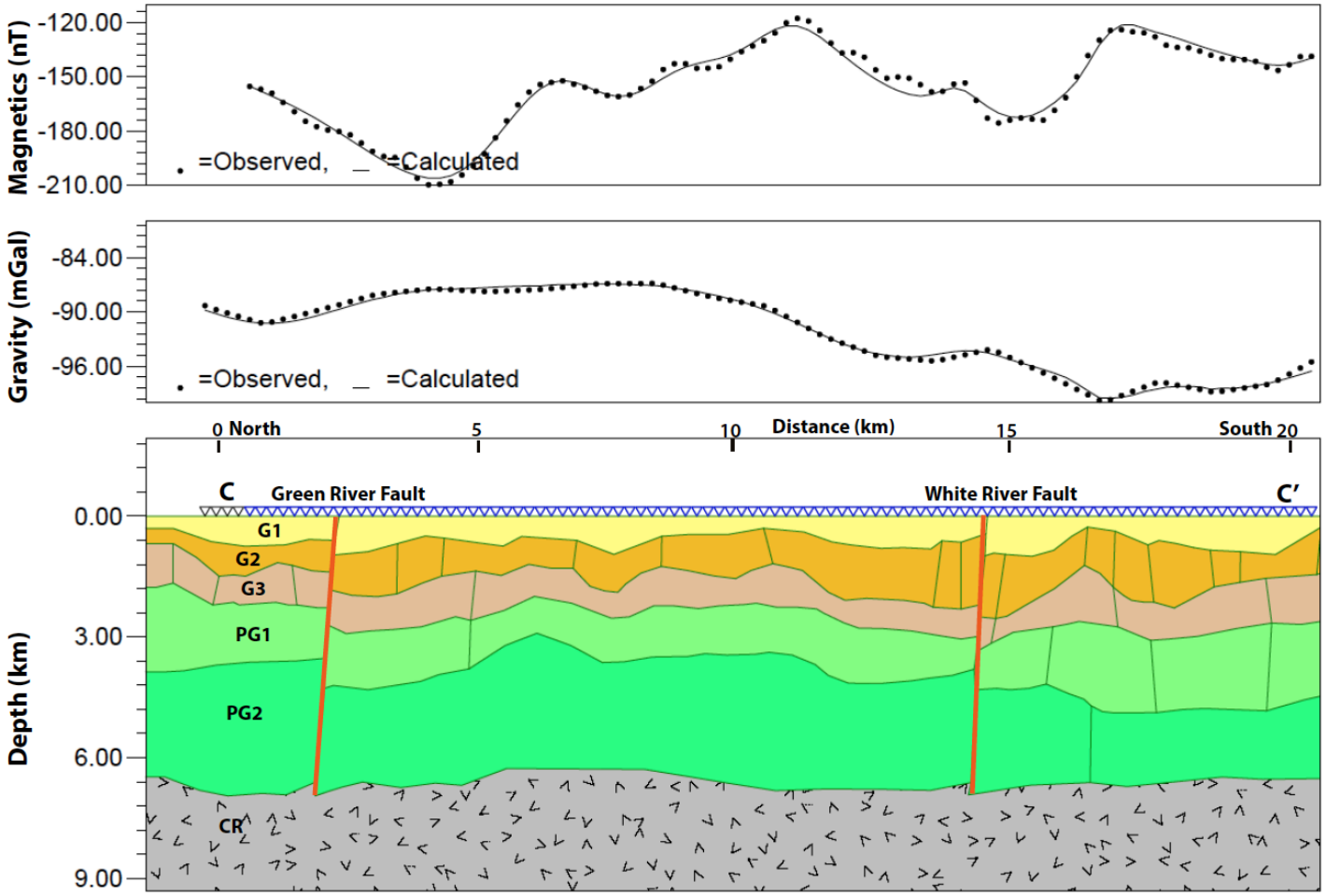


Figure 21. Gravity and magnetic profile C-C′. Abbreviations: G1=Glacial and post-glacial strata 1, G2=Glacial and post-glacial strata 2, G3=Glacial and post-glacial strata 3, P1= Puget Group 1, P2= Puget Group 2, CR= Crescent Formation, red lines= fault locations.

## Gravity and Magnetic Model: A-A′ Profile

Gravity and magnetic data for profile A-A′ are modeled by 6 subsurface bodies (Figure 19). Well data is extremely sparse and only extends to roughly 3 km in depth thus provide only constraints to the uppermost, younger sedimentary units. Gravity highs (-70.1 mGal on the west and -72.2 mGal to the east) are seen at both ends of the profile transect and correspond to bedrock exposures seen at the basin margins. The observed gravity is the lowest (-99.74 mGal) in the center of the curve representing the center of the basin. All the values contained within A-A′ are negative.

The observed magnetic curve for A-A′ is much more complex than the gravity curve, reflecting undulations associated with shorter-wavelength features. From the eastern end of the observed magnetic values decrease from -73.5 nT to -197.25 nT in the central portion of the cross-section. A small rise (up to -178 nT) in the magnetic curve occurs right at 6 km in the model, followed by a decrease to -200 nT, and then rapidly increases up to -116.5 nT. This steep, sharp increase in the observed magnetic values occur near the center of the basin, at the same location where the lowest anomaly values occur on the observed gravity curve. The observed magnetic curve continues to increase, undulating as it approaches the end of the profile. At roughly 20 km, a steep, but small increase from -94.1 nT to -38.28 nT in the magnetic values occurs. This “spike” in the magnetic curve coincides with a mapped exposure of the Tertiary Puget Group. The Franklin fault crosses the profile at the western edge of the exposed Puget group body. The Franklin fault is a strike-slip fault with about 1,000 feet of right lateral displacement (Vine, 1969). The Puget Group is mostly non-marine to marginal marine volcanic sedimentary rocks that underlie the young glacial sediments. In several locations, however, the Puget Group rock unit crops out along river cuts and eastern margin of the Muckleshoot basin.

The upper, Quaternary, glacial and post-glacial units are shown up to 3 km thick below profile A-A′. These glacial sediments are subdivided into three units, each with slightly varying densities and magnetic susceptibilities (Table 2). The two Puget Group units, both Tertiary, non-marine volcanic sedimentary rock formations, are roughly 3 km thick at the center of the basin. Near the eastern margin of the basin, however, the Puget Group is 5 to 6 km thick and crops out at the surface. The entire basin is modeled as approximately 7.5 km thick and is underlain by the dense, marine basalts of the Crescent Formation.

The most noticeable feature within the observed magnetic curve in A-A′ is the small bump followed by a steep increase in values around the 6 km mark on the profile. To accommodate this change, a south-verging thrust fault offsetting all six units within the basin was included at the peak of the magnetic high at the 10 km mark along the profile. This accommodation places the Puget Group units closer to the surface along the fault plane.

## Gravity and Magnetic Model: B-B′ Profile

Profile B-B′, located in the northern portion of the basin, shows an observed gravity curve quite similar to A-A′. The observed gravity curve in B-B′ displays a concave up shape with the gravity highs being on the two ends of the profile and the lowest values being in the center (Figure 20). The observed gravity is the highest (-62.13 mGal) at the western end of the profile. The lowest values (-96.6 mGal) coincide with the center of the basin. All observed gravity values along the curve are negative.

The western end of B-B′ records a magnetic value of -114.15 nT and decreases as the eastward along the profile towards the center of the basin. At about the midway point of the

profile (~12 km), a small spike occurs in the observed magnetics, which is then followed by a trough and then a steep, rapid increase from -170.21 nT to -99.6 nT. This steep change in the curve shares a pronounced similarity to that seen in the A-A′ profile. The increase in magnetics occurs at the same location at which the gravity curve shows the lowest measured readings along the profile. The observed magnetic curve slowly increases to -81.60 nT near the 20 km mark, but then dramatically decreases at the eastern extent of the profile to -207.45 nT. The profile does not cross any exposed geologic units at the surface other than the Quaternary sediments that cover the study area.

Similar to A-A′, the subsurface for B-B′ was modeled as having six geologic units, five of which make up the sedimentary basin. The three glacial and post-glacial sedimentary units reach a maximum combined thickness of 3 km, thinning towards the basin margins. The Puget Group Formation is divided into two separate units to account for the difference in sediment type Table 1). The top of the Puget Group beneath profile B-B′ is found between 2 to 3 km depth and reaches a maximum thickness of 4 km near this eastern part of the basin. The basin sediments reach a depth of approximately 7.5 km and are underlain by the Crescent Formation, which forms the basement.

At roughly the 15 km mark along the profile, the observed magnetic curve indicates a small rise followed by a slight dip and then a steep increase of more than 50 nT. This signature is very similar to that was observed along profile of A-A′. To accommodate this change, a steep, south-verging thrust fault was placed into the subsurface, offsetting all units within the basin. A small splay of the main fault offsets the upper two quaternary glacial units, which compensated for the small rise in magnetics to the west of the main fault signature.

## Gravity and Magnetic Model: C-C′ Profile

Gravity and magnetic profile C-C′ is oriented from north to south through the central part of the basin and intersects profiles A-A′ and B-B′ near the midpoint of each (Figure 19). C-C′ was placed directly onto a north-south transect of gravity measurement locations collected along a north-south oriented highway (Figure 16). This transect is slightly west of the central gravity low and slightly perpendicular to the gradient near the northern portion of the profile.

The observed gravity curve for the north end of C-C′ shows a slight dip in gravity, which correlates with the western edge of the northern sub-basin. The observed gravity curve increases to the south and reaches a peak of -84 mGal directly above the gravity high seen subdividing the basin in Figure 16. As the profile reaches the southern sub-basin, the gravity curve decreases to a minimum of -100 mGal before it begins to rise as it approaches the southern boundary of the basin.

The observed magnetics data for C-C′ show two significant features of particular interest. The first feature occurs around 5 km from the north end of the profile where the magnetic values reach a low of -210 nT before steeply increasing to -160 nT. The observed curve continues to increase and peaks at -130 nT, near the center of the profile line. This peak is located just south of the gravity high ridge seen in the CBA map in map view (Figure 14). The observed magnetic values decrease over the next several kilometers along the profile, with a few small undulations in the curve. Around 17 km, near the intersection of profile A-A′, a steep increase (-170 nT to -140 nT) in magnetics values occur. Both of the steep increases along the profile are very similar in shape indicating that they are a similar structure or feature. Both of these jumps in magnetic

values also occur near the two east-west profiles A-A′ and B-B′. Both A-A′ and B-B′ showed similar steep increases in the observed magnetic curve near their intersections with C-C′.

C-C′ crosses through both sub-basins, which are imaged in profiles A-A′ and B-B′. The subsurface structure modeled in the two east-west profiles achieved minimal error percentages for the observed and calculated gravity and magnetic data curve matches. Due to this, the north and south side of C-C′ were modeled to show similar depths and thicknesses of the six subsurface units as they were in the previous two profiles. The Quaternary glacial sediment units are roughly 3 km thick in both the northern and southern sub-basin. The Puget Group unit depth is relatively consistent with a depth to top varying from 2.5 to 3 km and a maximum thickness of 4 km. The Crescent formation sits just over 7 km below the surface and is relatively horizontal across the length of the profile.

The observed magnetic curve for C-C′ contains similar characteristics to those seen in profiles A-A′ and B-B′, where the two thrust faults occur. This suggests that the thrust faults modeled in the two east-west profiles also intersect C-C′ affecting the curve in a similar fashion. Within C-C′, the northern most thrust fault offsets all 6 units and records roughly 1 km of offset. The southern most thrust fault observable along A-A′ also offsets all 6 subsurface units but is showing 1.5 km of vertical displacement.

# 5. DISCUSSION

## Muckleshoot basin

The new three intersecting profiles modeled in this study provide insight into the Muckleshoot basin and illuminate several previously identified structures within and adjacent to the basin. The Muckleshoot basin was identified in earlier work as a broad, isolated gravity low east of the Puget Sound, with a northwest-trending gravity high "saddle" subdividing the basin into two sub-basins. Gravity maps prepared for this study identify the basin boundaries defined by a sharp contrast in high and low anomaly values (Figure 11 and 13). The dimensions of the basin are approximately 40 km north - south and 20 km east to west. The total area of the northern sub-basin is roughly 250 $km^2$ while the sub-basin to the south is 450 $km^2$. Subsurface models indicate the northern sub-basin sediments are 7.65 km deep before contacting the Crescent Formation basement rock. The models display sediments reaching 7.10 km within the sub-basin to the south.

The Complete Bouguer anomaly map (Figure 11) shows a northwest-trending, gravity high lineation that subdivides basin into two. Gravity profile C-C′ intersects this lineation from north to south within the basin boundaries. Although the observed gravity curve does reach its maximum anomaly value at the location at which the profile intersects the gravity high, there is no observed peak noticeable within the gravity curve to indicate a subsurface feature. The observed magnetic data in profile C-C′ has a pronounced peak near the gravity high ridge seen in map view. Based on the modeling results, this magnetic high could possibly be caused by a lithology change beneath the surface rather than a fault. The observed peak of the magnetic curve at the center of the sub-basins differs from the crests and troughs seen where faults are believed to cross the profile lines.

In the late Eocene, the Puget Lowland was dominated by a deltaic system depositing sediments into, at that time, the Pacific coastal plain. The massive delta system, known as a bird-foot complex, consisted thick sequences of localized topset interdistributary deposits and large multistory distributary channel deposits oriented perpendicular to the depositional strike. (Buckovic, 1979). During the early Oligocene, volcanism began to rapidly increase in the region due a shift in the subduction of the Farallon plate beneath North America. This increase in volcanism began to quickly deposit much more volcanic-rich sediments on top of the Eocene Puget Delta, completely covering what was in place (Buckovic, 1979). The general northwest-southeast trend of magnetic anomalies seen in the TFA map could be dictated by volcanic-rich Upper Puget Group Formation sediments deposited in channels or lobes of a deltaic fan. The sediments within this unit could cause a magnetic high due to the percentage of mafic minerals within the sediments deposited.

Observed gravity anomaly values at the base of each sub-basin are within 2 mGal (-99.28 mGal in southern sub-basin and -97.38 mGal in the northern). Depth to basement is 0.5 km deeper in the northern sub-basin. In a recent seismic reflection study, the Tacoma basin, west of the Muckleshoot, was observed as having low velocity rocks deeper in the northern portion as well (vanWagoner et al. 2002). This trend of asymmetric-shaped basins in the area is likely due to the regional north-south compression as Washington collides with the Canadian buttress.

**White River Fault**

Gravity and magnetic profiles A-A′ and C-C′ show evidence of some sort of structure beneath the surface causing the observed magnetic curves to rapidly increase over a short distance along the profile. This jump in magnetics occurs along profile A-A′ relatively close to the projected intersection with the White River fault following its current mapped trajectory into the basin (Figures 20, 21, and 22). To the southeast of the basin, the White River fault has been mapped as a steep, south-verging thrust fault that appears to be on strike with the active Tacoma fault, also a south-verging thrust fault (Brocher et al., 2001; Pratt et al., 1997). The shape of this anomaly could be attributed to: (1) a higher magnetic susceptibility unit to the east brought closer to the surface along a more vertical fault plane, or (2) a lower angle thrust fault that doubles the vertical section on the northside. Both scenarios would cause a magnetic high on the thrusted hanging wall side of the reverse fault. Previous studies have shown that the WRF southeast of the Muckleshoot is steeply dipping (Box et al., 2003), therefore the first scenario may be more consistent with this observation; however, fault dips often vary along strike. (Blakely et al., 2007) conducted a gravity and magnetic survey southeast of the basin focusing on the WRF and zones of alteration associated with the fault zone. They consistently found that magnetic anomaly values decrease from north to south across the WRF. Profiles A-A’ and C-C’ show a magnetic high on the east and northeast side as would be suspected with the WRF crossing in a northwest-southeast trend.

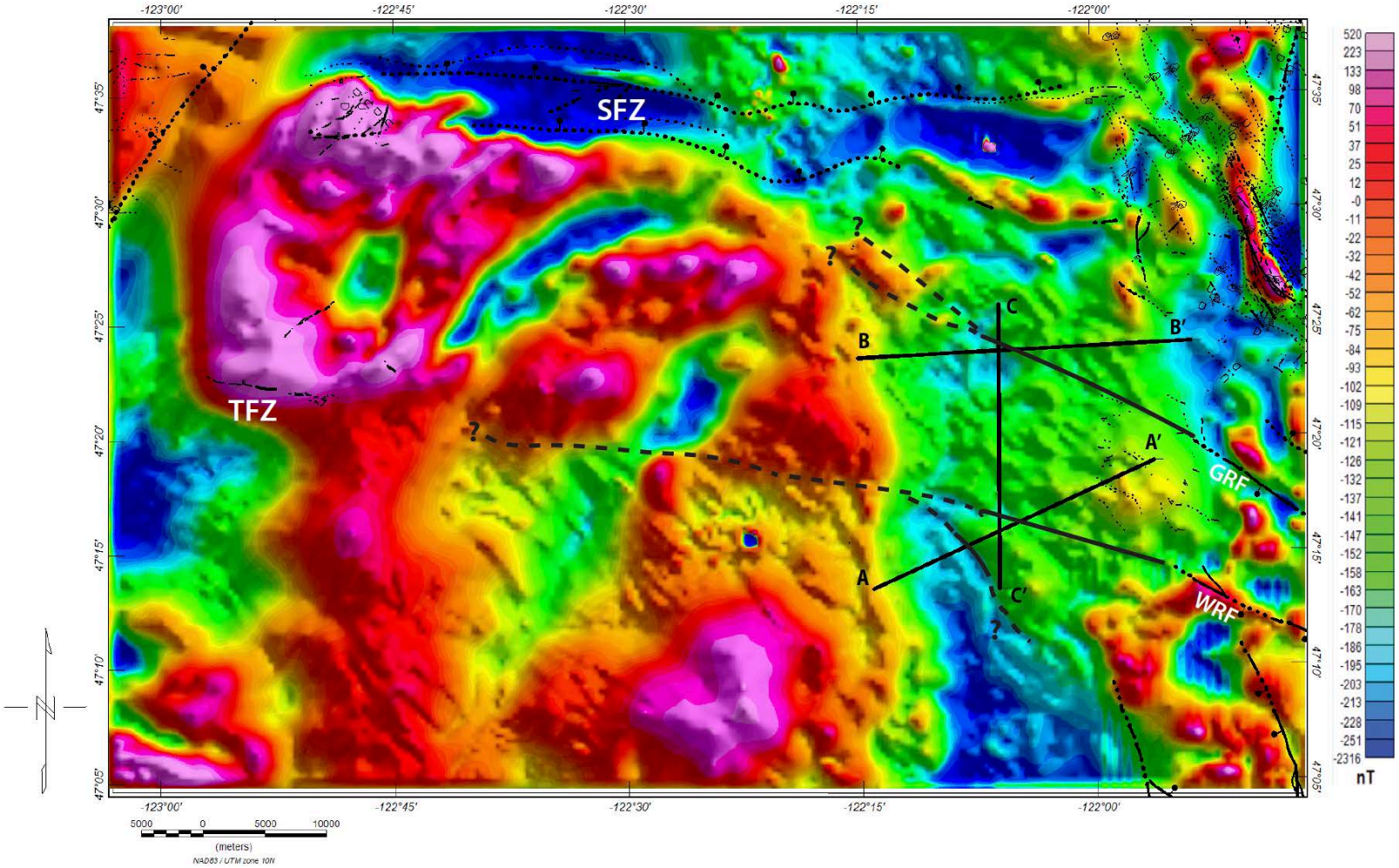


Figure 22. TFA magnetic map with modeled fault locations plotted. Solid black lines=fault trajectories based on models in this study. Dashed black lines=inferred fault locations. Solid blue lines=faults. Abbreviations: WRF=White River fault, GRF=Green River fault.

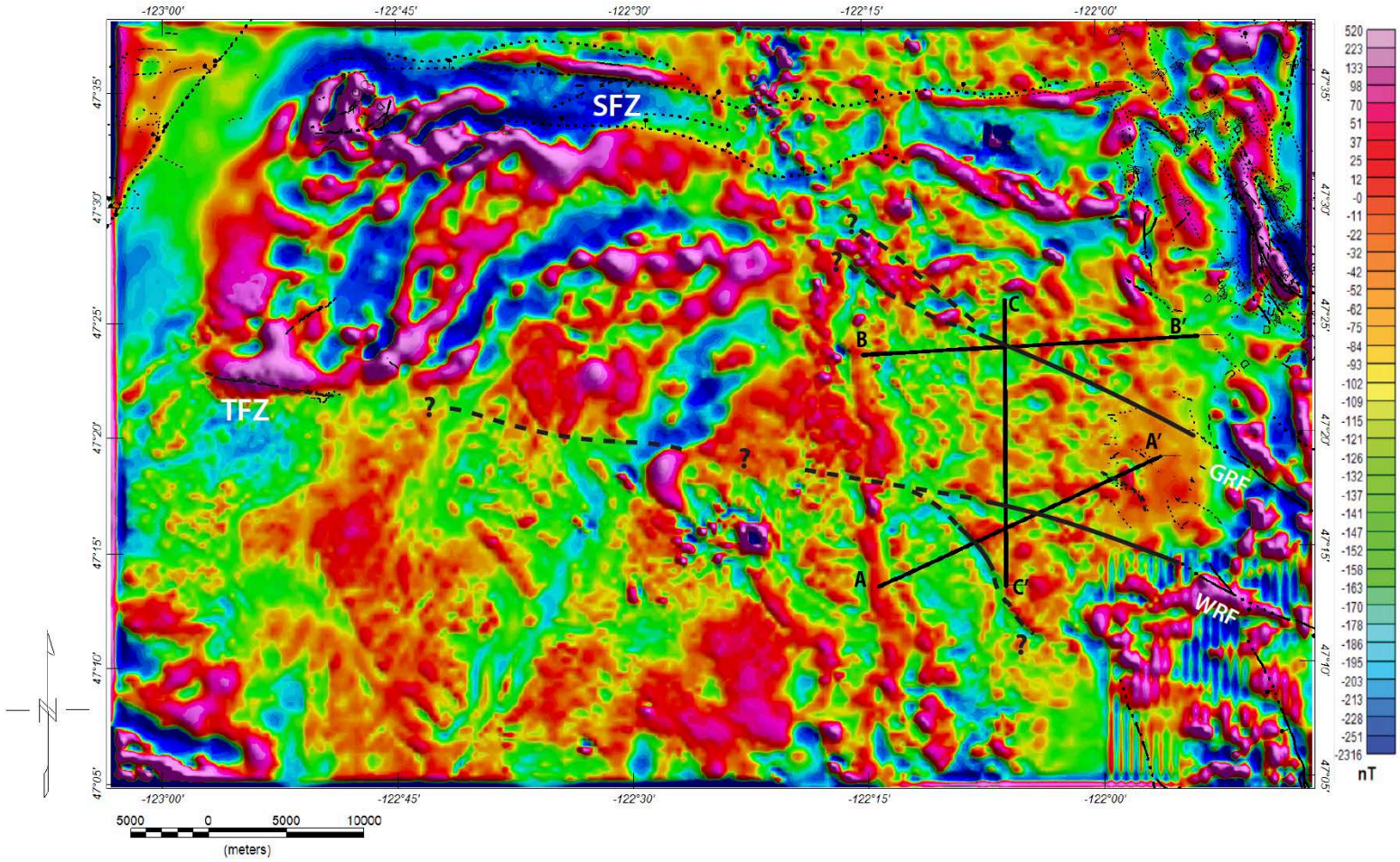


Figure 23. Vertical derivative magnetic map with modeled fault locations plotted. Solid black lines=fault locations based on models in this study. Dashed black lines=inferred fault locations. Solid blue lines=faults. Abbreviations: SFZ=Seattle fault zone, TFZ=Tacoma fault zoneWRF=White River fault, GRF=Green River fault.

The same variation in the magnetic curve appears in the observed magnetics within profile C-C′. This magnetic high anomaly occurs along C-C′ at the intersection with profile A-A′. This magnetic high observed on both profiles (A-A′ and C-C′) is likely the WRF

West of the profiles, the geometry of the WRF is still uncertain; however, the models indicate that the WRF bends slightly west, aligning with a splay of the Tacoma fault (Figures 21, 22, and 23). Additional work on the western margin of Muckleshoot basin could provide the last piece of evidence that the two faults are, in fact, connected.

## Green River Fault

The observed magnetic data along profile B-B′ depicts a similar crest and trough shape as seen in A-A′. This feature correlates with the strike of the Green River fault, mapped east of the basin. Like the WRF, the GRF is a steep, south-verging reverse fault that is unable to be traced through the surficial Quaternary sediments covering the basin. Because both faults mimic the same sense of movement and dip angle, the expression of the GRF in the observed magnetics as it intersects profile B-B′ should look very similar to what is seen as the WRF crosses A-A′ (Figures 20, 21, 22). Figures 17 and 18 show how similar the curves look in each modeled profile. The GRF can be seen crossing profile C-C′ as well, slightly north of where it crosses B-B’.

To the east of the basin, the GRF is mapped along the surface for approximately 20 km but is discontinuous within the Miocene-aged Fifes Peak Formation (Blakely et al., 2007). The similarity of the GRF to the WRF suggests that the two are may be related. One possibility is that the GRF is a step fault parallel to the WRF. Another possible scenario is that the Tacoma

fault and WRF are genetically related, creating one extensive fault zone, and the GRF is a splay branching off of the primary fault system.

## An Interactive Fault System

Blakely et al. (2011) and Reidel and Campbell (1989) argue that based on magnetic anomalies, the WRF appears to cut through the Cascade Mountains and merge with the Umtanum Ridge fault northeast of Cleman Mountain, north of Naches, Washington. If their hypotheses are correct, the WRF is connected to a fault zone that stretches for roughly 100 km into central Washington. Models within this study suggest that the WRF crosses the Muckleshoot basin and aligns with the Tacoma fault. If the WRF and Tacoma fault do, in fact, merge as one extensive fault zone, the fault system would exceed 185 km in length, stretching from the Olympic Mountains to Umtanum Ridge (Figure 10a).

A fault zone of these dimensions would dramatically affect seismic hazard assessment calculations for the Tacoma-Seattle metropolitan area. If each fault is segmented, movement from one section along the fault zone could trigger subsequent ruptures along the fault at great distances.

# 6. CONCLUSIONS

Gravity and magnetic data analyzed in this study delineates the boundaries of the Muckleshoot basin as 40 km long and 20 km wide, reaching a maximum depth of 7.65 km. The basin is segmented by a northwest-southeast trending gravity high into two sub-basins. Subsurface models show the northern sub-basin is 0.5 km deeper than the sub-basin to the south, but is roughly 200 $km^2$ smaller in total area. Although this gravity high is a prominent feature in both the CBA and the vertical derivative gravity maps, it does not appear as a distinctive feature in the magnetic data. This suggests that the gravity high is associated with deep structure. Gravity and magnetic models do not conclude that either the WRF or GRF is associated with the gravity high segmentation.

Results from the gravity and magnetic modeling of the Muckleshoot basin indicate that the WRF does cross the southern portion of the basin, then bends westward and aligns with the Tacoma fault. Similarly, the GRF crosses the northern portion of the basin, exhibiting the same south-verging reverse sense of movement as the WRF. Both faults show a sense of movement consistent with that of the Tacoma fault zone raising the possibility that these faults zones are genetically related. Subsurface models indicate that both the WRF and GRF offset all 6 lithological units within the Muckleshoot basin, including Holocene-aged post-glacial sedimentary units. This suggests that both faults are currently active and in agreement with previous studies.

Future work should focus on the western side of the Muckleshoot basin to determine the geometry of the projected WRF as it approaches the Tacoma fault system to the west. Additional data, such as new seismic surveys or acquisition of existing industry data would provide greater insight into these relations. Although the GRF has been identified in previous work, this study suggests that it deserves more attention as a potential seismogenic structure.

# REFERENCES


Babcock, R.S., Burmester, R.F., Engebretson, D.C., and Warnock, A., 1992, A rifted margin origin for the Cresent basalts and reltated rocks in the Northern Coast Range Volcanic Province, Washington and British Columbia: Journal of Geophysical Research, v. 97, no. B5, p. 6799-6821.

Blakely, R.J., 1995, Potential theory in gravity and magnetic applications: New York, Cambridge University Press, p.1-441.

Blakely, R.J., Wells, R.E., and Weaver, C.S., 1999, Puget Sound aeromagnetic maps and data, U.S. Geological Survey Open File Report, 99-514.

Blakely, R.J., Wells, R.E., Weaver, C.S., and Johnson, S.Y., 2002, Location, structure, and seismicity of the Seattle fault zone, Washington; evidence from aeromagnetic anomalies, geologic mapping, and seismic-reflection data, Geological Society of America Bulletin, v. 114, no. 2, p. 169-177.

Blakely, R.J., John, D.A., Box, S.E., Berger, B.R., Fleck, R.J., Ashley, R.P., Newport, G.R., and Heinemeyer, G.R., 2007, Crustal controls on magmatic-hydrothermal systems: A geophysical comparison of White River, Washington, with Goldfield, Nevada, Geosphere; April 2007, v. 3, no. 2, p. 91–107.

Blakely, R.J., Sherrod, B.L., Weaver, C.S., Wells, R.E., Rohay, A.C., Barnett, E.A., and Knepprath, N.E., 2011, Connecting the Yakima fold and thrust belt to active faults in the Puget Lowland, Washington: Journal of Geophysical Research, v. 116, B07105, 33 p.

Blakely, R.J., Sherrod, B.L., Weaver, C.S., Wells, R.E., and Rohay, A.C., 2014, The Wallula fault and tectonic framework of south-central Washinton, as interpreted from magnetic and gravity anomalies, Tectonophysics, 624-625, p. 32-45.

Blunt, D.J., Easterbrook, D.J., and Rutter, N.W., 1987, Chronology of Pliestoncene sediments in the Puget Lowland, Washington, Washington Division of Geology and Earth Resources Bulletin 77, p. 321-353.

Bring, U.S., Song, J., and Bucknam, R.C., 2006, Rupture models for the A.D. 900-930 Seattle fault earthquake from uplifted shorelines, Geology, v. 34, p. 585-588.

Brocher, T. M., T. Parsons, R. J. Blakely, N. I. Christensen, M. A. Fisher, R. E. Wells, and the SHIPS Working Group, 2001, Upper crustal structure in Puget lowland, Washington: Results from 1998 seismic hazards investigation in Puget Sound, Journal of Geophysical Research, 106, 13,541–13,564.

Bucknam, R.C., Hemphill-Haley, E., and Leopold, E.B., 1992, Abrupt uplift within the past 1700 years at southern Puget sound, Washington, Science, New Series, vol. 258, no. 5088, p. 1611-1614.

Buckovic, W.A., 1979, The Eocene deltaic system of west-central Washington, Pacific Coast Paleogeography Symposium 3: Cenozoic Paleogeography of the Western United States, p. 147-163.

Bustin, M.M., Clowes, R.M., Monger, J.W.H, and Murray Journeay, J., 2013, The southern Coast Mountains, British Columbia: new interpretations from geological, seismic reflection, and gravity data, Canadian Journal of Earth Science, vol. 50, p. 1033-1050.

Campbell, N.P., 1989, Structural and stratigraphic interpretation of rocks under Yakima fold belt, Columbia basin, based on recent surface mapping and well data, Geological Society of America Special Papers 239, p. 209-222.

Danes, Z.F., Bonno, M.M., Brau, E., Gilham, W.D., Hoffman, T.F., 1965, Geophysical investigation of the southern Puget Sound area, Washington, Journal of Geophysical Research, v. 70, no. 22, p. 5573-5580.

Dater, D., Metzger, D., and Hittelman, A., 1999, Land and Marine Gravity CD-ROMs, U.S. Department of Commerce, National Oceanic and Atmospheric Administration, National Geophysical Data Center, Boulder, CO.

Finn, C., Phillips, W.M., and Williams, D.L., 1991, Gravity anomaly and terrain maps of Washington, scale 1:500000 and 1:1,000,000, U.S. Geological Survey Geophysical Investigation Map, GP-988.

Fuller, C.W., Willet, S.D., and Brandon, M.T., 2006, Formation of forearc basins and their influence on subduction zone earthquakes, Geology, v. 34, p. 65-68,

Hagstrum, J.T., Booth, D.B., Troost, K.G., Blakely, R.J., 2002, Magnetostratigraphy, paleomagnetic correlation, and deformation of Pleistocene deposits in the south central Puget Lowland, Washington, Journal of Geophysical Research, v. 107, no. B4, 2079.

Harvey, M.K., Sherrod, B.L., Nelson, A.R., and Brocher, T.M., 2008, Earthquakes generated from bedding plane-parallel reverse faults and above active wedge thrust, Seattle fault zone, Geological Society of American Bulletin, v. 120, p. 1581-1597.

Haugerud, R.A., Harding, D.J., Johnson, S.Y., Harless, J.L., and Weaver, C.S., 2003, High-Resolution LiDAR Topography of the Puget Lowland, Washington, Geological Society of America Today, v. 13, no. 6, p. 4-10.

Hooper, P.R., and Conrey, R.M., A model for the tectonic setting of the Columbia River basalt eruptions, in Volcanism and Tectonism in the Columbia River Flood-Basalt Province, Geological Society of America Special Paper 239, edited by S.P. Reidel, and P.R. Hooper, pp. 293-306, 1989.

Johnson, S.Y., Potter, C.J., Miller, J.J., Armentrout, J.M., Finn, C., and Weaver, C.S., 1996, The southern Whidbey Island fault: an active structure in the Puget Lowland, Washington, Geological Society of America Bulletin, v. 108, no. 3, p. 334-354.

Johnson, S.Y., Dadisman, S.V., Childs, J.R. and Stanley, W.D., 1999, Active tectonics of the Seattle fault and central Puget Sound, Washington - implications for earthquake hazards, Geological Society of America Bulletin, v. 111, no. 7, p. 1042-1053.

Johnson, S.Y., Nelson, A.R., Personius, S.F., Wells, R.E., Kelsey, H.M., Sherrod, B.L., Okumura, K., Koehler, R., Witter, R.C., Bradley, L.A., and Harding, D.J., 2004, Evidence for late Holocene earthquakes on the Utsalady Point Fault, northern Puget Lowland, Washington, Bulletin of the Seismological Society of America, v. 94, no. 6, p. 2299– 2316.

Johnson, S. Y., R. J. Blakely, W. J. Stephenson, S. V. Dadisman, and M. A. Fisher, 2004, Active shortening of the Cascadia forearc and implications for seismic hazards of the Puget Lowland, Tectonics, v. 23, TC1011.

Kelsey, H.M., Sherrod, B.L., Blakely, R.J., and Haugerud, R.A., 2012, Holocene faulting in the Bellingham forearc basin: Upper-plate deformation at the northern end of the Cascadia subduction zone, Journal of Geophysical Research, v. 117, B03409.

Liberty, M.L., 2007, Seismic reflection imaging across the eastern portions of the Tacoma fault zone, U.S. Geological Survey Project Award Number: # 07HQGR0088.

Libery, M.L., and Pratt, T. L., 2008, Structure of eastern Seattle fault zone, Washington State: new insights from seismic reflection data, Bulletin of the Seismological Society of America, v. 98, no. 4, p. 1681-1695.

Mace, C.G., and Keranen, K.M., 2012, Oblique fault systems crossing the Seattle Basin: geophysical evidence for additional shallow fault systems in the central Puget Lowland, Journal of Geophysical Research, v. 117, B03105.

McCaffrey, R., King, R.W., Payne, S.J., and Lancaster, M., 2013, Active tectonics of northwestern U.S. inferred from GPS-derived surface velocities, Journal of Geophysical Research: Solid Earth, v. 118, p. 709-723.

Mullineaux, D.R., 1979, Geology of the Renton, Auburn, and Black Diamond quadrangles, King County, Washington, Geological Survey Professional Paper 672.

Pezzopane, S. K., and Weldon, R. J., 1993, Tectonic role of active faulting in central Oregon: Tectonics, v. 12, p. 1140–1169.

Pratt, T.L., Johnson, S., Potter, C., Stephenson, W., Finn, C., 1997, Seismic reflection images beneath Puget Sound, western Washington State: The Puget Lowland thrust sheet hypothesis, Journal of Geophysical Research, v. 102, no. B12, p. 469-27, 489.

Raisz, E., 1945, The Olympic Wallowa lineament; American Journal of Science, v. 243, p. 479–485.

Sherrod, B.L., Blakely, R.J., Weaver, C.S., Kelsey, H.M., Barnett, E., Liberty, L., Meagher, K.L., and Pape, K., 2008, Finding concealed active faults: Extending the southern Whidbey Island fault across the Puget Lowland, Washington, Journal of Geophysical Research, v. 113.

Tabor, R.W., Frizzell, V.A., Jr., Booth, D.B., and Waitt, R.B., 2000, Geologic map of the Snoqualmie Pass 30 × 60′ quadrangle, Washington: U.S. Geological Survey Geologic Investigations Series Map I2538, scale1:100,000.

Taylor, J.P., 2013, A Gravity Study of Holocene Active Structures in the Puget Lowland of Washington State (Master's thesis). Retrieved from Dissertations and Theses Database.

U.S. Census Bureau, 2010, Seattle-Tacoma-Bellevue, WA - Population Change for Metropolitan and Micropolitan Statistics Areas in the United States and Puerto Rico. [PDF]. Retrieved http://www.census.gov/population/www/cen2010/cph-t/CPH-T-2.pdf.

Van Wagoner, T.M., Crosson, R.S., Creager, K.C., Medema, G.F., Preston, L.A., Symons, N.P., and Brocher, T.M., 2002, Crustal structure and relocated earthquakes in the Puget Lowland, Washington from high resolution seismic tomography, Journal of Geophysical Research, v. 107 (B12), 2381.

Vine, J. D., 1969, Geology and Coal Resources of the Cumberland, Hobart, and Maple Valley quadrangles, King County, Washington, Geological Survey Professional Paper 624.

Wshington Division of Geology and Earth Resources, 2014, Surface geology, 1:24,000--GIS data, June 2014: Washington Division of Geology and Earth Resources Digital Data Series DS-10, version 1.0.